

Alma Mater Studiorum Università di Bologna  
Archivio istituzionale della ricerca

Electrosynthesis and characterization of Layered Double Hydroxides on different supports

This is the final peer-reviewed author's accepted manuscript (postprint) of the following publication:

*Published Version:*

Musella E., Gualandi I., Giorgetti M., Scavetta E., Basile F., Rivalta A., et al. (2021). Electrosynthesis and characterization of Layered Double Hydroxides on different supports. APPLIED CLAY SCIENCE, 202, 1-12 [10.1016/j.clay.2020.105949].

*Availability:*

This version is available at: <https://hdl.handle.net/11585/790490> since: 2021-01-22

*Published:*

DOI: <http://doi.org/10.1016/j.clay.2020.105949>

*Terms of use:*

Some rights reserved. The terms and conditions for the reuse of this version of the manuscript are specified in the publishing policy. For all terms of use and more information see the publisher's website.

This item was downloaded from IRIS Università di Bologna (<https://cris.unibo.it/>).  
When citing, please refer to the published version.

(Article begins on next page)

This is the final peer-reviewed accepted manuscript of:

**Musella, E.; Gualandi, I.; Giorgetti, M.; Scavetta, E.; Basile, F.; Rivalta, A.; Venuti, E.; Corticelli, F.; Christian, M.; Morandi, V.; Tonelli, D. Electrosynthesis and Characterization of Layered Double Hydroxides on Different Supports. Applied Clay Science 2021, 202, 105949.**

The final published version is available online at:  
<https://doi.org/10.1016/j.clay.2020.105949>

#### Terms of use:

Some rights reserved. The terms and conditions for the reuse of this version of the manuscript are specified in the publishing policy. For all terms of use and more information see the publisher's website.

*This item was downloaded from IRIS Università di Bologna (<https://cris.unibo.it/>)*

***When citing, please refer to the published version.***

# Electrosynthesis and characterization of Layered Double Hydroxides on different supports

Elisa Musella <sup>1</sup>, Isacco Gualandi <sup>1</sup>, Marco Giorgetti <sup>1</sup>, Erika Scavetta<sup>1</sup>, Francesco Basile<sup>1</sup>, Arianna Rivalta <sup>1</sup>, Elisabetta Venuti <sup>1</sup>, Franco Corticelli <sup>2</sup>, Meganne Christian <sup>2</sup>, Vittorio Morandi <sup>2</sup> and Domenica Tonelli <sup>1,\*</sup>

<sup>1</sup> Dipartimento di Chimica Industriale “Toso Montanari”, Università di Bologna, Viale Risorgimento 4, 40136 Bologna, Italy

<sup>2</sup> Istituto per la Microelettronica e i Microsistemi (IMM), Consiglio Nazionale delle Ricerche (CNR), Sede di Bologna, via Gobetti 101, 40129 Bologna, Italy

\* Correspondence: domenica.tonelli@unibo.it; Tel.: (+39 051 2093667)

**Abstract:** Thin films of Al, and Co or Ni based Layered Double Hydroxides (LDH) have been electrochemically deposited on four different supports (Grafoil, Toray Carbon Paper, Carbon Cloth and Nickel Foam) through a potentiostatic or a potentiodynamic approach. The obtained films have been fully characterized to compare their properties in dependence on the different deposition techniques and substrates. Finally, the Grafoil support modified with a Ni /Al-LDH has been employed as cathode in combination with a Grafoil anode modified with poly(3,4-ethylenedioxythiophene)-poly(styrenesulfonate) (PEDOT:PSS) also electrosynthesized, in order to develop an all-binder-free hybrid supercapacitor as a proof of concept to demonstrate the applicability in the field of energy storage.

**Keywords:** Layered Double Hydroxides; electrosynthesis; hybrid supercapacitors; conductive support

## 1. Introduction

Electrochemical energy storage is a key technology in the field of the energy that would otherwise be wasted. Although batteries have been successfully used in light-duty vehicles, hybrid platforms for trucks and buses require storage and delivery of currents much higher than those which can be accommodated by batteries. Electrochemical capacitors (ECs), unlike batteries, can operate at high charge and discharge rates over an almost unlimited number of cycles and enable energy recovery in heavier-duty systems. (Miller and Simon, 2008) Therefore, ECs, also called supercapacitors, have attracted increasing interest for their capability to deliver high power density in a very short time, excellent cyclability, and ability to store more charge than conventional capacitors. They accumulate charge by adsorption of electrolyte ions onto the

27 surface of electrode materials, whereas in the case of pseudocapacitors the capacitance arises from fast and  
28 reversible redox reactions (of Faradaic nature) occurring at or close to the electrode surface. (Vlamidis et al.,  
29 2017)

30 Environmental sustainability is also essential if large-scale production and diffusion are planned. Since all  
31 harmful substances should be avoided, new eco-friendly devices are proposed in the literature, where the  
32 organic solvent is replaced with water or/and the binder employed for electrode preparation is  
33 eliminated.(Conte et al., 2004) Research is thus focusing on supercapacitors which are binder-free, safe,  
34 composed of earth abundant elements and able to work in aqueous electrolyte.

35 In this scenario, layered double hydroxides (LDH) are promising materials, able to satisfy these  
36 requirements. They are synthetic lamellar hydroxides with two or more kinds of metal cations in the main  
37 layers and hydrated interlayer domains containing anionic species. (He et al., 2006)

38 The basic layer structure of a LDH is based on that of brucite  $[Mg(OH)_2]$ , typically associated with small  
39 polarizing cations and polarizable anions. It consists of magnesium ions surrounded octahedrally by  
40 hydroxide ions. These octahedral units form infinite layers by edge-sharing, with the hydroxide ions sitting  
41 perpendicular to the plane of the layers. The layers then stack on top of one another to form the three-  
42 dimensional structure. (Meyer and Sauvage, 2005)

43 The basic structure of a LDH may be derived by substitution of a fraction of the divalent cations  $M(II)$  in a  
44 brucite lattice by trivalent cations  $M(III)$  so that the layers acquire a positive charge, which is balanced by  
45 intercalation of anions (and, usually, water) among the layers. It is the possibility of varying the identity and  
46 relative proportions of the di- and trivalent cations as well as the identity of the interlayer anions that gives  
47 rise to the large variety of materials having the general formula  $[M^{II}_{1-x}M^{III}_x(OH)_2]^{x+}[A^{n-}]_{x/n} \cdot m H_2O$ . (Meyer  
48 and Sauvage, 2005)

49 Concerning the cations, the only restriction is the size of the radius of  $M(II)$  and  $M(III)$  ions. Their ionic radii  
50 should not differ much from those of the natural LDH ( $Mg^{2+}$  and  $Al^{3+}$ , respectively) so that they may be  
51 accommodated in the octahedral sites of the brucite-like layers. For this reason, good candidates are divalent  
52 cations such as  $Ni^{2+}$ ,  $Mg^{2+}$ ,  $Ca^{2+}$ ,  $Mn^{2+}$ ,  $Co^{2+}$ ,  $Cu^{2+}$  or  $Zn^{2+}$  together with trivalent cations such as  $Al^{3+}$ ,  $Co^{3+}$ ,  
53  $Fe^{3+}$  or  $Cr^{3+}$ . (Cavani et al., 1991) The ratio  $x$  between  $M(II)$  and  $M(III)$  is also an important feature. It has

54 been reported to fall in the range  $0.1 \leq x \leq 0.5$ , but pure LDH phases only exist for  $0.2 \leq x \leq 0.33$ . For  $x$   
55 values outside this range, compounds with different structures are obtained. (Khan and O'Hare, 2002)

56 By virtue of their structural tunability, LDH and some of their nanocomposites can be employed in an  
57 impressive number of applications, such as electrocatalysts, (Benito et al., 2015) sensors, (Scavetta et al.,  
58 2014a; Gualandi et al., 2015), pseudo-capacitors (Zhang et al., 2015; Zhang and Wei, 2019), drug delivery  
59 systems, (Asiabi et al., 2019) and for intercalation chemistry. (Khan and O'Hare, 2002) The interesting  
60 properties of these materials include large surface areas, anion exchange capacities (2–3 meq/g), comparable  
61 to those of the classical anion exchange resins, recovering of the layered structure after thermal  
62 decomposition, and low cytotoxicity. (Cavani et al., 1991)

63 In the literature, several synthetic techniques are reported for LDH preparation. The most commonly  
64 encountered involve the simple coprecipitation (Nalawade et al., 2009) and hydrothermal methods, (Ogawa  
65 and Asai, 2000) but others include urea hydrolysis, (Adachi-pagano et al., 2003) glycine assisted  
66 hydrothermal synthesis (Prevot et al., 2009) and reconstruction. (Erickson et al., 2005) The major drawbacks  
67 of these syntheses are the long time needed for the reaction to occur and the poor adhesion to the support  
68 material when the LDH is used as a coating, such as in electrochemical applications. (Miyata, 1983) In  
69 particular, when a powder is obtained, it is necessary to formulate the electrode with inactive components,  
70 e.g. a binder, which are typically insulators. These processes greatly devalue and affect the final  
71 performances.

72 For all these reasons, a fascinating synthetic procedure is electrodeposition, since it allows for both the  
73 synthesis and simultaneous modification of the electrode surface without using a binder. Moreover, the  
74 problems related to adhesion are overcome.

75 Since 2004 our group has been working on the electrodeposition of LDH (Scavetta et al., 2004) and, up to  
76 date, the potentiostatic approach is certainly the most commonly used method for the direct modification of  
77 conductive substrates with LDH. (Scavetta et al., 2004; Gualandi et al., 2011; Vlamidis et al., 2017) The  
78 synthesis of LDH by electrodeposition is usually carried out in a solution containing the nitrates of the  
79 bivalent and trivalent ions, applying to the electrode a cathodic potential which promotes the reduction of

80 nitrates and water molecules. The reactions involved consume  $H^+$  and produce  $OH^-$  near the electrode  
81 surface, so the local pH increases leading to the LDH precipitation. (Scavetta et al., 2004, 2012, 2014b)

82 Of course, some drawbacks exist also for this strategy. Firstly, the concentration gradients arising during the  
83 synthesis hinder a fine control of the M(II)/M(III) ratio in the deposited material, which rarely is the same of  
84 the synthetic bath, especially when a long potential pulse is applied. (Bernardi et al., 2016; Yang et al., 2017)

85 Secondly, the characterization cyclic voltammogram (CV) does not always display a reproducible signal as  
86 in the redox active couple. As to both issues, our group (Gualandi et al., 2019; Musella et al., 2019b) has  
87 recently demonstrated that a potentiodynamic approach, where the deposition is performed by CV in the  
88 cathodic side, provides a reproducibility of the deposit which is much better than the one achieved with  
89 either galvanostatic or potentiostatic methods. (Musella et al., 2019a)

90 Also conducting polymers (CPs) are a class of materials largely employed in energy storage field.  
91 They offer the advantages of low cost, great charge density and often display good intrinsic  
92 conductivity. Among CPs, poly(3,4-ethylenedioxythiophene)-poly(styrenesulfonate) (PEDOT:PSS)  
93 is very interesting due to the easy processability. It is promising as a charge storage material since  
94 the oxygen atoms that have unfilled valence shells allow for high doping levels. (Hareesh et al.,  
95 2016) Moreover, it is possible to obtain the polymer through an electrochemical synthesis which is  
96 quite a delicate process but offers interesting advantages like the use of low monomer  
97 concentrations, short duration, and good control of the film thickness. (Vlamidis et al., 2015)

98 In the present work, we report a systematic comparison between the electrochemical synthetic  
99 protocols for LDH on four different electrode substrates (three of which are carbon based, whilst the  
100 fourth is a Nickel Foam), performing a full characterization of the deposits from a chemical,  
101 morphological, and electrochemical point of view. Finally, one of the supports, i.e. Grafoil modified  
102 with a Ni /Al LDH, has been tested in combination with an anode modified with PEDOT:PSS also  
103 electrochemically synthesized as a proof of concept for the development of an all-binder-free hybrid  
104 supercapacitor that works in aqueous electrolyte with high performances.

## 105 **2. Materials and Methods**

### 106 **2.1 Instrumentation**

107 The electrochemical experiments were carried out in a conventional three electrode cell or in a two-terminal  
108 device. Electrode potentials were measured with respect to an aqueous saturated calomel electrode (SCE) or  
109 a mercury/mercury oxide one (Hg/HgO). A Pt wire was used as the counter electrode. The curves were  
110 recorded by means of a CH Instruments Mod. 660C, controlled by a personal computer via CH Instruments  
111 software.

112 The morphology, structure, and chemical compositions of the LDH films were investigated by Field  
113 Emission-Scanning Electron Microscopy (FE-SEM) using a LEO 1530 ZEISS instrument equipped with  
114 Schottky emitter, operated at an acceleration voltage variable from 5 to 15 keV, and Everhart-Thornley and  
115 In-lens detectors for secondary electrons imaging. Energy Dispersive X-ray Spectroscopy (EDS)  
116 measurements were performed with an Oxford INCA system equipped with a 30 mm<sup>2</sup> Silicon Drift Detector.

117 Raman spectra were recorded with the Renishaw System RM1000. The spectrometer was coupled to a Leica  
118 DMLM microscope equipped with 50x, 20x and 5x objectives which allowed, with the 50x objective, a  
119 nominal spatial resolution < 2 μm in xy and 4 μm in z. The excitation wavelength was from an argon laser  
120 tuned at 514.5 nm. The output power of the laser was around 25 mW, but when needed the light intensity  
121 impinging on the film was reduced by neutral density filters to avoid sample damage.

## 122 **2.2 Preparation of chemically modified electrodes**

123 Cleaning the electrode is a critical step to achieve a well adherent coating. Four different substrates have  
124 been employed (Grafoil, Toray Carbon Paper, Carbon Cloth, Nickel Foam).

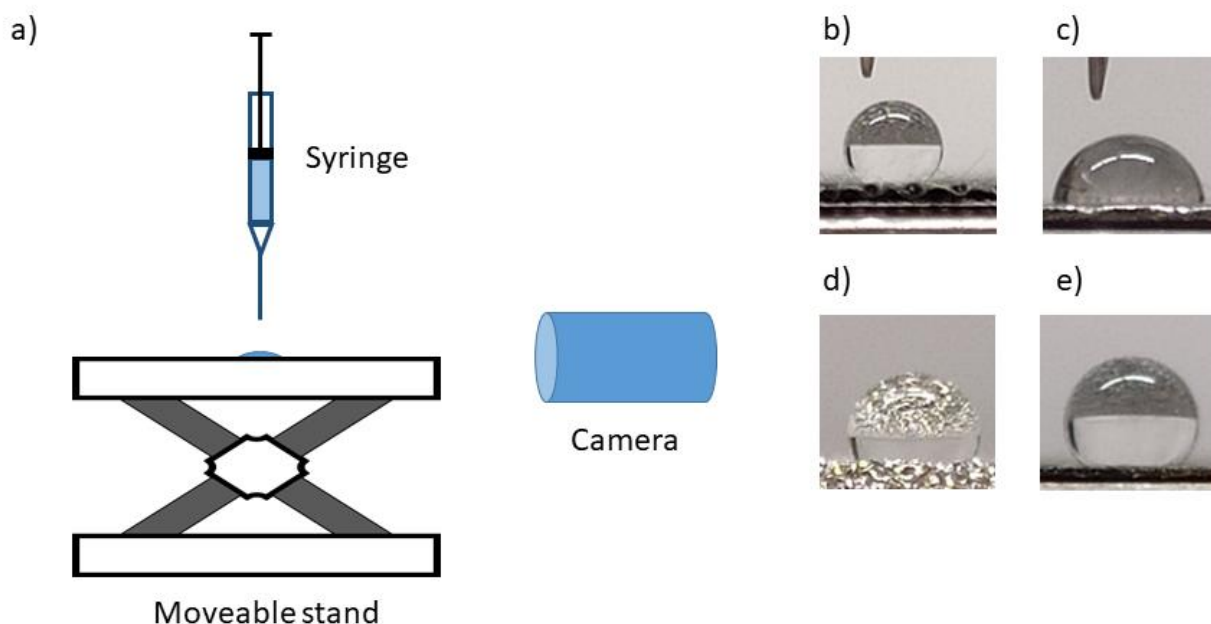
125 Grafoil (G) was provided by VED, the bulk density is 1.12 g/mL, the resistivity is  $7.33 \cdot 10^{-4} \Omega \text{ cm}$  and the  
126 carbon content is established at 99.5%, while the ash content at 0.5%. Carbon Cloth (CC) and Toray Carbon  
127 Paper (TC) were provided by Quintech. Carbon Cloth has a bulk density 1.75g/mL, a resistivity of 85  
128 mΩ cm and a tensile strength of 10 N/cm. Toray Carbon Paper has a good porosity (78% empty space), a  
129 resistivity of 80 mΩ cm, and a tensile strength of 50 N/cm. Nickel Foam (NiF) was provided by Xiamen Tob  
130 New Energy Technology Co, and has high porosity (97% empty space) and a resistivity of 7.6 μΩ m.

131 The fabrication starts by cutting the material in the desired geometry and dimensions before the polishing  
132 treatment. The electrodes must have the shape of a 3x1cm<sup>2</sup> rectangle, with the active area of 1x1 cm<sup>2</sup>

133 delimited by Teflon tape. Depending on the substrate, the procedures adopted for the cleaning are listed  
134 hereby:

- 135 • G: the electrode was rinsed in ethanol for 10 min and then dried to constant weight.
- 136 • CC: the electrode was sequentially rinsed for 5 min in the following solvents: acetone, ethanol, and  
137 distilled water. Finally, it was dried to constant weight.
- 138 • TC: the electrode was rinsed in ethanol for 10 min and then dried to constant weight.
- 139 • NiF: the electrode was immersed in acetone for 10 min at 50°C under sonication, then in distilled  
140 water for 10 min at 50°C, again under sonication, and finally dried to constant weight.

141 The contact angle of each substrate was statically measured by a home-made set-up (Fig. 1a) which is  
142 composed of a photo-camera, a stage with a variable height, a syringe mounted on a support. A droplet was  
143 carefully deposited on the investigated substrate by the syringe which was positioned above the sample  
144 surface. The photo-camera was aligned to the substrate and captured an image of the droplet profile and the  
145 substrate. (Fig. 1b-e) The contact angle was measured by using a dedicated software.



146

147 **Figure 1:** a) Home-made set up for the statistical measure of contact angle. Picture recorded for Carbon Cloth (b),  
148 Grafoil (c), Nickel Foam (d) and Toray Carbon Paper (e).



Subsequently, the LDH films were deposited on the electrode surface by cathodic reduction of a freshly prepared 0.03 M solution containing Co or Ni and Al (from nitrate salts) at a molar ratio of 3:1. Two electrochemical approaches were used for the synthesis of LDH: a potentiostatic and a potentiodynamic one aiming to a comparison when applied to different geometry and porosity conditions. All parameters were optimized to achieve the highest reproducibility of the deposition and are reported in Tables 1 and 2 for the potentiodynamic (2 potential cycles) and potentiostatic depositions, respectively. After the modification, all the modified electrodes were immediately rinsed with water.

**Table 1:** Selected parameters (potential window and scan rate) for the potentiodynamic syntheses (indicated as \_D in the text)

	<b>G</b>	<b>CC</b>	<b>TC</b>	<b>NiF</b>
<b>Ni/Al</b>	-1.3 – 0.0 V 25 mV/s	-1.3 – 0.0 V 30 mV/s	-1.4 – 0.0 V 30 mV/s	-1.3 – 0.0 V 30 mV/s
<b>Co/Al</b>	-1.3 – 0.0 V 30 mV/s	-1.3 – 0.0 V 30 mV/s	-1.4 – 0.0 V 30 mV/s	-1.3 – 0.0 V 30 mV/s

158

**Table 2:** Selected parameters for the potentiostatic syntheses (indicated as \_S in the text)

	<b>G</b>	<b>CC</b>	<b>TC</b>	<b>NiF</b>
<b>Ni/Al</b>	-1.3 V 30s	-1.2 V 30s	-1.2 V 30s	-1.2 V 30s
<b>Co/Al</b>	-1.3 V 30s	-1.2 V 30s	-1.2 V 30s	-1.2 V 30s

160

As to the anode, PEDOT:PSS has been chosen as active material. The starting deposition solution contained 0.1 mM polystyrene sulfonate (PSS) and 10 mM solution of 3,4-Ethylenedioxythiophene (EDOT). The

163 mixture of EDOT and PSS was stirred for 45 min until complete dissolution. The deposition was carried out  
 164 by means of an electrochemical approach, using 25 cycles of CVs from 0.00 V to +1.20 V at 100 mV/s.  
 165 The specific capacitance ( $C_s$ ) can be calculated using following equations. From the CV curves,

$$166 \quad a) \quad C_s = \frac{\int I dV}{Sv\Delta V}$$

167 where the integral represents the area of the CV curve,  $v$  (V/s) is the scan rate,  $\Delta V$  (V) is the potential  
 168 window, and  $S$  (cm<sup>2</sup>) is the effective area. The given values are the average of the data obtained for all the  
 169 investigated scan rates. From the galvanostatic charge/discharge (GCD) curves,

$$170 \quad b) \quad C_s = \frac{I\Delta t}{S\Delta V}$$

171 where  $I$ (A) and  $\Delta t$ (s) are the discharging current and time, respectively.

## 172 **3. Results and Discussion**

### 173 **3.1. Characterization of supports**

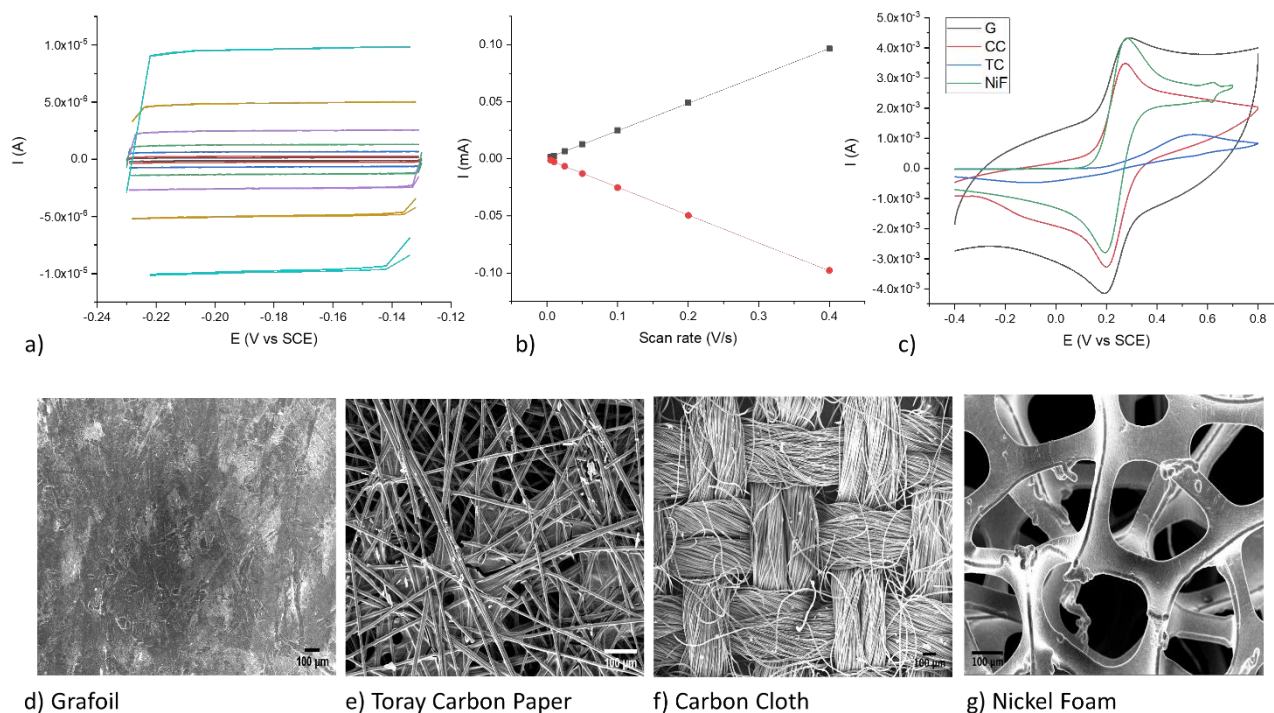
174 Four different electrode supports were investigated in this work, namely G, TC, CC and NiF. These materials  
 175 have been selected due to their widespread use in the field of energy storage. In particular, our aim was to  
 176 propose a strategy to promptly prepare modified electrodes able to be applied in the electrochemical field  
 177 without the employment of strong treatments or harmful substances. We decided just to wash the surface to  
 178 remove dirt accumulated during the materials storage. Of course, the lack of pre-treatment can highly affect  
 179 the electrodeposition process, and therefore, the following characterizations which have been carried out.  
 180 First of all, the electrochemically active areas (ECSA) were estimated by two approaches in order to  
 181 highlight the two phenomena that may affect the redox processes. The former method estimates the double-  
 182 layer capacitance of the system from CV in 1 M NaOH, employing the protocol introduced by McCrory et  
 183 al. (McCrory et al., 2013, 2015). Currents are recorded in CVs at potentials close to the open circuit value  
 184 (OCP) (Figure 2a which refers to TC, is shown as an example). The charging current,  $I_c$ , is equal to the  
 185 product of the double layer electrochemical capacitance ( $C_{DL}$ ) and the scan rate ( $v$ ):  $I_c = vC_{DL}$ .  $C_{DL}$  is  
 186 calculated as the slope of the line obtained by plotting  $I_c$  versus scan rate  $v$ . (Figure 2b) The ECSA value is  
 187 obtained by dividing  $C_{DL}$  by the specific capacitance of the electrolyte ( $C_s$ ), which is reported by McCrory

188 for 1 M NaOH ( $0.040 \text{ mF cm}^{-2}$ ). In all investigated cases, the same geometrical area ( $A_g$ ) has been  
189 considered to perform a proper comparison. The highest ECSA was registered for Grafoil, with a value of 5  
190 followed by TC, NiF and CC with 3, 0.45 and  $0.4 \text{ cm}^2$ , respectively. These capacitance measurements  
191 estimate all the active area only at the electrode-solution interface.

192 Therefore, ECSA was also estimated using a redox probe (ferricyanide) by means of the Randle-Sevcik  
193 equation in order to better simulate the conditions for which an electron transfer process takes place, using a  
194 diffusion coefficient equal to  $0.72 \cdot 10^{-5} \text{ cm}^2/\text{s}$  according to literature (Konopka et al.). Fig. 2c shows the CVs  
195 recorded in 0.1 M KCl containing 5 mM ferricyanide at the different substrates.

196 TC exhibit the smallest area ( $0.52 \text{ cm}^2$ ) which is again lower than the geometric area, and the highest value is  
197 observed for Ni Foam ( $2.37 \text{ cm}^2$ ). G and CC also display a high area ( $1.56$  and  $1.25 \text{ cm}^2$ ), respectively.  
198 Moreover, the CVs show that the response of ferricyanide is quasi-reversible for NiF, G and CC as checked  
199 from the separation between anodic and cathodic peaks of the redox probe, which is near enough to the  
200 theoretical value for a one-electron process. However, this is not true for TC. It is worth mentioning that G  
201 has a huge capacitive contribution, which can be helpful in the development of hybrid capacitors.

202 The different data obtained by the two methods are explained considering that ferricyanide ions access  
203 differently to the active surface. Therefore, the porosity and the structure of the different systems play a key  
204 role in the evaluation of the area resulting from the use of ferricyanide Faradaic current.



205

206 **Figure 2:** a) Double-layer capacitance measurements to determine ECSA for TC support using voltammetry in 1 M  
 207 NaOH. Cyclic voltammograms were recorded at the following scan rates: 0.005 (black line), 0.01 (red line), 0.025 (blue  
 208 line), 0.05 (green line), 0.1 (purple line), 0.2 (dark yellow line), and (light blue line) 0.8 V/s. (b) Cathodic (red circle)  
 209 and anodic (black square) currents measured at the OCP value plotted as a linear function of scan rate. (c) CVs obtained  
 210 in 0.1 M KCl containing 5 mM ferricyanide at the different substrates (d-g) SEM images of bare supports (same scale  
 211 bar): (d) G (e) TC (f) CC (g) NiF.

212

213 Figures 2 (d-g) show the micrographs of the bare substrates. Grafoil displays a wrinkled surface, which is  
 214 typical of graphite sheets (Fig. 2d). In fact, it is produced from natural or synthetic flaky graphite by means  
 215 of an oxidizing agent in order to form an interlayer composite. Subsequently, a high temperature heating  
 216 abruptly produces the material rapid expansion. Defects, as wrinkles and folded graphite layers, are clearly  
 217 shown (bright lines in the image) (Morishita, 2011) as well as impurities and contaminants (round shaped  
 218 bright particles).

219 Toray Carbon Paper is made of carbon fibers stacked and inter-crossed together (Figure 2e). Its structure is  
 220 very complex: three different areas are displayed, where two solid regions and voids appear. One solid  
 221 region consists of long, thin randomly distributed fibers. The other one looks like a thin sheet binding the

222 fibers of the paper. These fibers are supposed to be good electron conductors; hence, they are typically  
223 employed to transport electrons to and from the layers. (Zamel et al., 2009)

224 Carbon Cloth is a woven textile material consisting of carbon fibers oriented in two directions, as shown in  
225 Figure 2f. It can be described as a twill weave and it looks like a wicker basket with good conductivity.  
226 (Brasquet et al., 2000)

227 Figure 2g shows that the Nickel Foam has a 3D, cross-linked grid structure, with considerable and uniform  
228 wrinkles on its surface. This porous skeleton should, in principle, provide electrolyte accessible channels for  
229 ion transportation, and shorten the distance for ion diffusion. (Yang et al., 2008)

230 Moreover, the contact angle was evaluated. The ability to evaluate the wetting of solids by liquids is an  
231 important feature for many applications, including the capability to coat a surface. Wettability is obtained by  
232 measuring the contact angle formed between a liquid drop and a solid surface. The calculated values are  
233 reported in Table 3, and confirm that the most hydrophilic support is Grafoil, whereas the most hydrophobic  
234 one is Carbon Cloth.

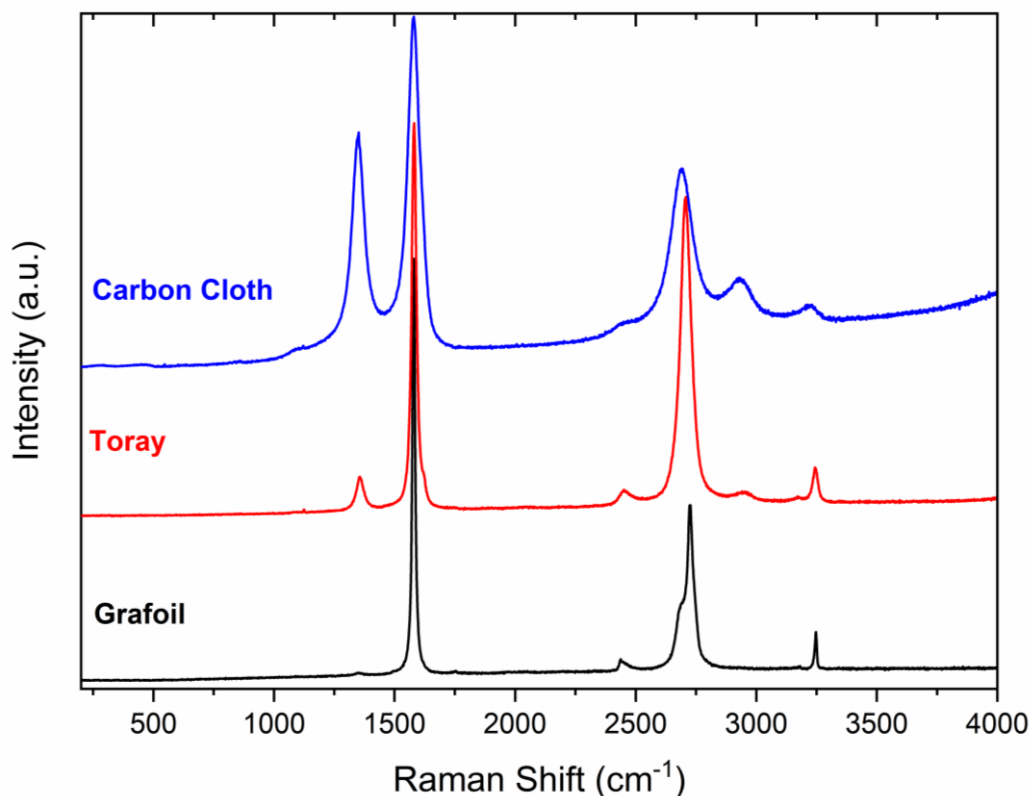
235 **Table 3:** Values of contact angle for the analyzed supports

	<b>G</b>	<b>CC</b>	<b>NiF</b>	<b>TC</b>
<b>Value (°)</b>	$82 \pm 2$	$140 \pm 1$	$110 \pm 7$	$127 \pm 6$

236

237 Finally, the substrates were analyzed by means of Raman spectroscopy (Fig. 3). Clearly, the Raman  
238 spectrum was not recorded for Ni Foam since the pure metal does not show Raman signals. The technique is  
239 widely used in literature to characterize carbon-based materials among which Grafoil, Carbon Cloth and  
240 Toray Paper. The spectra display the bands typical of these carbon-based materials (Jorio et al. 2016, Ferrari  
241 et al. 2013, Su et al. 2009, Cuesta et al. 1994). In particular, the Grafoil spectrum corresponds to that of  
242 highly ordered graphite, with the intense G band at  $1580 \text{ cm}^{-1}$ , and other narrow bands at 2452, 2725 (with a  
243 shoulder at 2692) and  $3248 \text{ cm}^{-1}$ , assigned to overtones or combinations. Note that the D band is virtually  
244 absent. Such a band appears with low intensity in the Toray's spectrum, together with the weak overtone at  
245  $2939 \text{ cm}^{-1}$ , normally detected in defected graphite. Otherwise, Toray exhibits features very similar to Grafoil.

246 An intense D band is instead observed at  $1350\text{ cm}^{-1}$  for the Carbon Cloth substrate, yielding a ratio  $I_D/I_G =$   
 247  $0.59$ , also accompanied by an increased intensity of the band near  $2940\text{ cm}^{-1}$  and a broadening of all features.  
 248 Clearly, this substrate is the one with more structural defects.

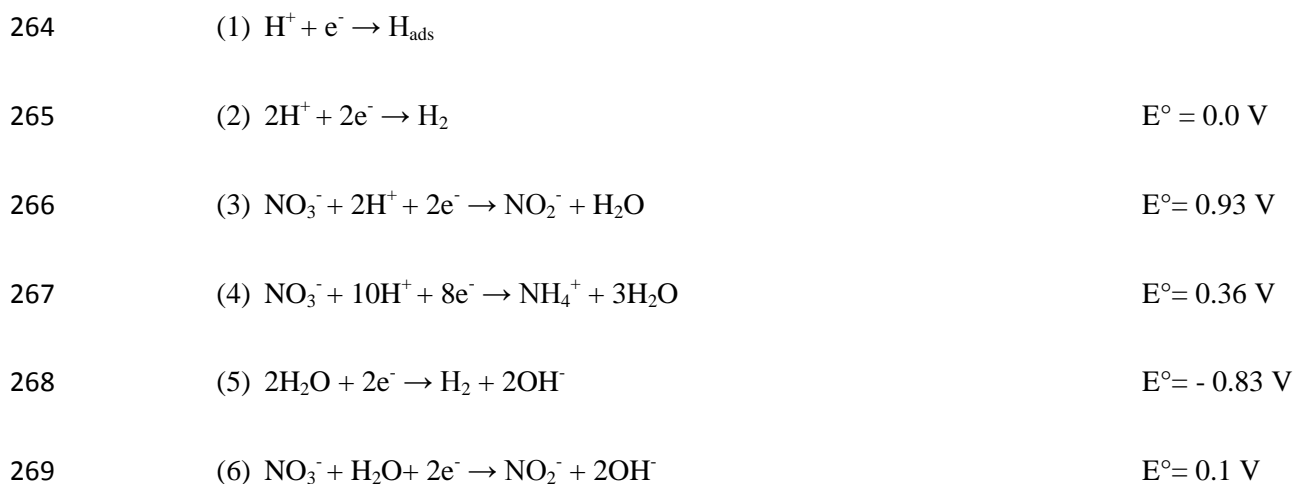


250  
 251 **Figure 3:** Raman spectra of Grafoil, Toray and Carbon Cloth substrates.

### 252 **3.2 Electrochemical deposition and characterization of LDH**

253 Independently of the synthetic approach chosen, the experimental conditions were varied in order to obtain  
 254 LDH films, which displayed the highest reproducibility, evaluated through CV characterization. The electro-  
 255 synthesis was carried out on three different carbonaceous materials and on Ni foam, and parameters such as  
 256 the scan rate and the potential window were investigated for the potentiodynamic approach, whilst only the  
 257 applied potential for the potentiostatic one. In the latter case, time was not considered as a variable and thus  
 258 was set at 30 s, because the concentration gradients hinder the control of cations molar ratio in the final  
 259 material when a long potential pulse is applied. (Bernardi et al., 2016)

260 The electrochemical synthesis was carried out by reduction of a nitrate solution of nickel or cobalt and  
 261 aluminum ions. It consists of several reactions that contribute to the precipitation of the LDH, next and on  
 262 the electrode surface. The reactions 1-6 cause the disappearance of  $H^+$  ions and/or the production of  $OH^-$   
 263 ions, which induce the pH increase necessary for the LDH precipitation: (Scavetta et al., 2014b)



270 A strong kinetic control dominates the nitrate reduction leading to a very complex multistep process, where  
 271 the rate of the electrochemical reaction strongly depends on the activity of the electrode surface. For  
 272 example, it was already reported (Gualandi et al., 2012) that the quality of the electrodeposited LDH films  
 273 can be highly affected by the pre-treatment performed on the Pt surface.

274 Two processes are involved in LDH precipitation: the nucleation and the growth of crystals, and the presence  
 275 of defects on the substrate surface can affect the rate of these processes. LDH precipitation involves the  
 276 following reagents:  $M(II)$ ,  $M(III)$ , and  $OH^-$ . The cations diffuse from the solution bulk to the electrode  
 277 surface, whereas  $OH^-$  ions are created at electrode surface and diffuse toward the solution bulk. An efficient  
 278 LDH electrosynthesis takes place when the hydroxide ions production compensates the  $OH^-$  removal by the  
 279 LDH precipitation. Considering these factors, even small variations of the electrode surface can significantly  
 280 affect the LDH deposition: therefore, a very robust procedure is necessary to obtain reproducible results.

281 As stated in the Materials and Methods Section, we tested two approaches and four supports in order to find  
 282 the best electrodeposition procedure:

283 1. **Potentiostatic deposition.** This is the most commonly employed procedure in the literature: it  
 284 is performed by applying a constant potential to the working electrode. It allows for the control

of both the system thermodynamics and kinetics through the overpotential. A process that should be avoided is water reduction because hydrogen evolution can damage the LDH film. However, the use of this approach does not ensure a fine control of the metal ratio. (Gualandi et al., 2019)

2. **Potentiodynamic electrodeposition.** With this approach, the deposition is stimulated by performing a cyclic voltammetry in the cathodic side. The most anodic potential is fixed far from the onset potential of deposition so to have enough time to restore the cation concentration close to the electrode surface by diffusion. It is possible to finely control the ratio of the metals in the deposited film. (Musella et al., 2019a)

The deposition curves recorded during the syntheses of the Co/Al and Ni/Al LDH are displayed in Figure 4. In all the studied cases, the highest current has been observed for the NiF support, independently of the LDH deposited, followed by CC, G and TC.

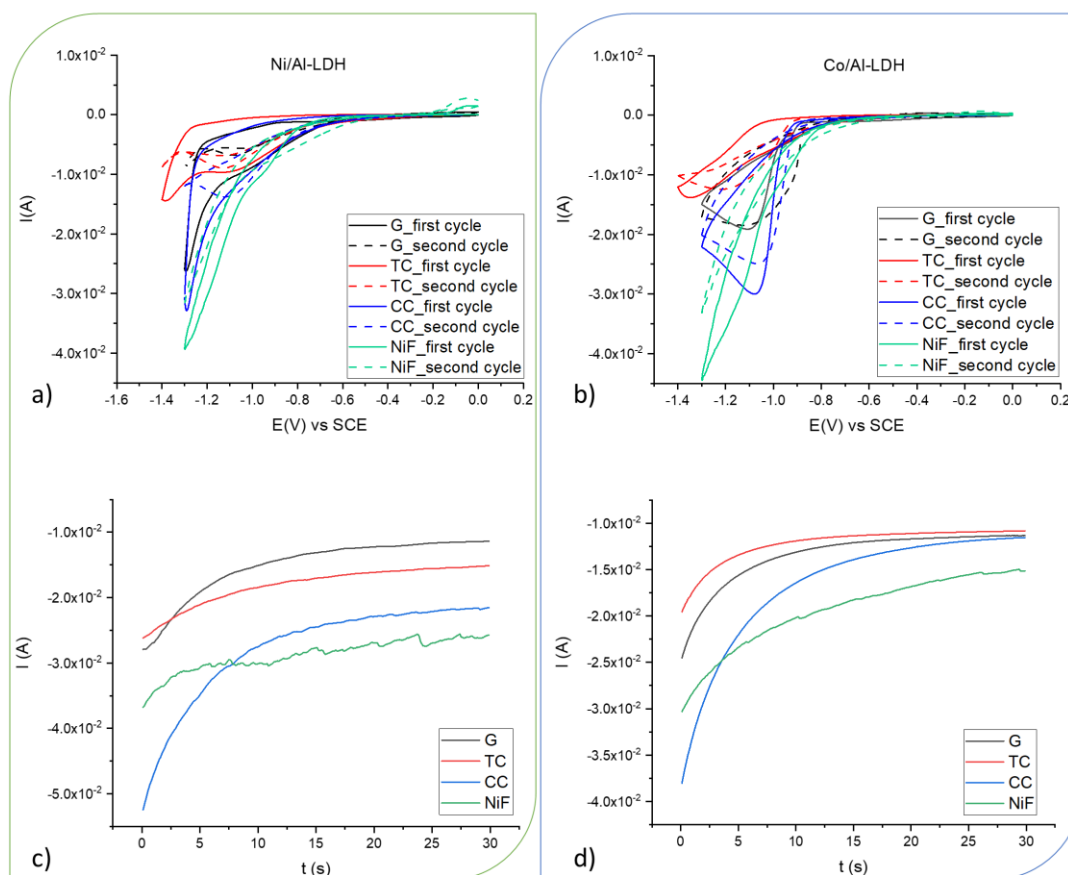




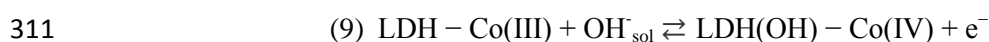
**Figure 4.** Comparison between the electrosynthetic approaches. CVs recorded during potentiodynamic syntheses of Ni/Al-LDH, (a) and of Co/Al-LDH (b). I vs time curve recorded during potentiostatic syntheses of Ni/Al-LDH (c) and of Co/Al-LDH (d). Parameters for these depositions are reported in Tables 1 and 2.

The reproducibility of the procedures was tested by evaluating the peak currents associated with the redox signal of metal centers, obtained by CV. The Ni/Al-LDH undergoes the following reaction (Figure 5a, b): (Yang et al., 2013; Gualandi et al., 2019)



The typical peaks, observed in the potential window between +0.35 and +0.6 V are related to the quasi reversible redox couple Ni(III)/Ni(II). The partial irreversibility is due to the oxidation of Ni(II) centers to Ni(III), characterized by a cooperative Jahn-Teller effect, which could induce a chemical/structural instability. (Cavani et al., 1991)

The Co/Al-LDH, instead, undergoes the following reactions (Figure 5c, d): (Totir et al., 2000)



The Co based LDH coating displays a broad feature due to the closeness of the formal potentials of the reactions (8) and (9) which hinders the resolution of the two peaks. Anyway, the behavior can be considered reversible since the ratio of the anodic to the cathodic charge of the feature is very close to 1.

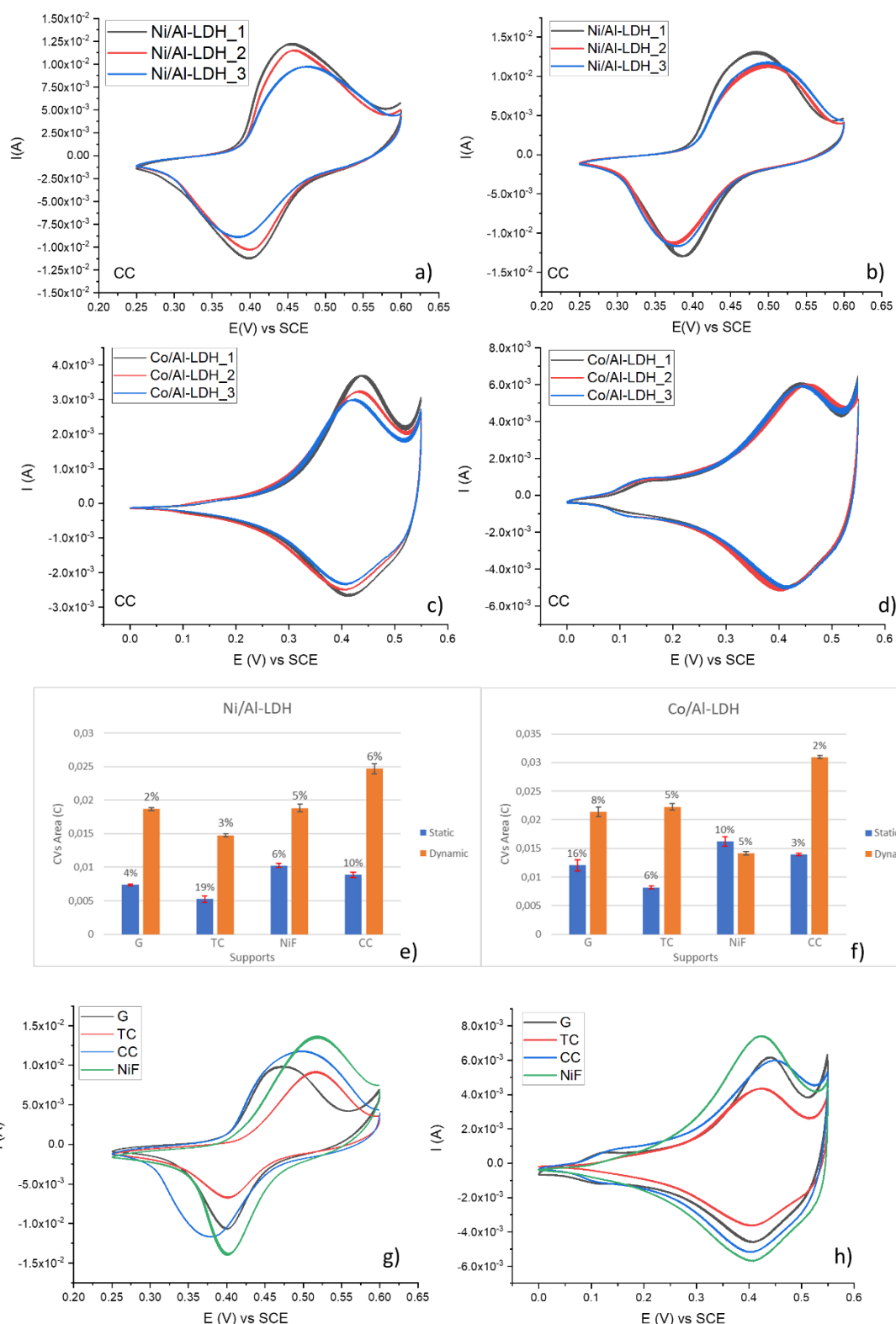
In particular, Figures 5a–d show the CVs relevant to the optimized procedures to obtain the best results in terms of reproducibility of the electrochemical signal for CC supports. The curves relevant to the other supports are reported in SI 1. The potentiostatic deposition exhibits the lowest robustness independently of the support adopted, as it does not allow for a fine control of the OH<sup>−</sup> production, and, consequently, of the amount of precipitated LDH. On the other hand, when the synthesis is performed by a potentiodynamic procedure, the results display good reproducibility with a relative standard deviation of the CV area which is generally below 5%, vs a value often higher than 10% for the potentiostatic synthesis (as displayed in figures 5 e, f). Moreover, the current intensities and CV areas recorded for the potentiodynamic syntheses are higher than those for the potentiostatic one, which means that a higher amount of material has been deposited.

Therefore, it is clear that the potentiodynamic approach is more satisfying in all the cases studied. In addition, it can be inferred that the reproducibility is mainly affected by the nature of the substrate and not by the nature of the bivalent cation present in the brucitic layers since a univocal trend is recognizable for both LDH. The effect of the substrate is again evident comparing the characterization signal of LDH (Figure 5 g,h). In the case of films obtained with the dynamic syntheses, which are shown in the figures, the same current trend recorded for the deposition curves is observed: the highest current intensities are measured for the NiF support independently of the LDH deposited, followed by CC, G and TC. Finally, it is possible to argue that the main contribution to the rate of the electrochemical reaction is due to the activity of the bare electrode surface, independently of the synthetic strategy adopted.

Finally, the average specific capacitance ( $C_s$ ) calculated from the CVs are reported in Table 4. It can be noticed that the most suitable systems to be tested in hybrid capacitors are those produced through the potentiodynamic synthesis on CC or G.

**Table 4.** Specific capacitance calculated from the CVs for all analyzed systems.

	$C_s$ (F/cm <sup>2</sup> )			
	<b>G</b>	<b>TC</b>	<b>NiF</b>	<b>CC</b>
<b>Ni_D</b>	1.2	0.8	1.1	1.4
<b>Co_D</b>	1.6	1.1	0.8	1.8
<b>Ni_S</b>	0.8	0.5	0.6	0.8
<b>Co_S</b>	0.8	0.4	0.9	0.7



338

339 **Figure 5.** CVs recorded at 10 mV/s in 0.1 M KOH for Ni-Al LDH and Co-Al LDH prepared with the two  
 340 electrosynthetic approaches onto CC supports. Ni/Al-LDH prepared by potentiostatic (a), and potentiodynamic (b)  
 341 protocols; Co/Al-LDH prepared by potentiostatic (c), and potentiodynamic (d) protocols. Numbers 1, 2 and 3 refer to  
 342 different electrodes in order to highlight the reproducibility of the synthetic procedure. Areas with relative error for

343 Ni/Al-LDH (e) and Co/Al-LDH (f). Comparison of the characterizations among supports for Ni/Al-LDH\_D (g) and  
344 for Co/Al-LDH\_D (h).

### 345 **3.3. Morphology of LDH**

346 The morphology of the LDH films has been investigated by means of FE-SEM (Figure 6).

347 As far as the LDH films are concerned, we can say that when the potentiodynamic approach is employed, the  
348 substrate is homogeneously covered, and no detachment of the film is highlighted in any case, viceversa if  
349 the potentiostatic synthesis is performed the deposit shows breakages and detachments.

350 When Grafoil is the support, a nanostructured film is obtained, which can be described as highly  
351 homogeneous and compact with a thickness of 0.8-1  $\mu\text{m}$  for the potentiodynamic synthesis, and of 500 nm  
352 for the potentiostatic one (Figure 6\_1b-e). In the case of Toray Carbon Paper (Figure 6\_2b-e) and Carbon  
353 Cloth (Figure 6\_3b-e), the classical desert rose structures are visible for both syntheses. However, in the case  
354 of 6\_2c and 6\_2e the morphology is not the same throughout the deposit (static synthesis) and, in particular,  
355 the substrate is not homogeneously covered. In all cases, the film is nanostructured with thicknesses ranging  
356 from 300 to a maximum of 500 nm. When Nickel Foam is employed as a substrate, a great variety of  
357 morphologies are recorded ((Figure 6\_4b-e). A “desert rose” like morphology appears only in the case of  
358 Co/Al LDH synthesized via the potentiostatic route while the potentiodynamic one gives rise to a film which  
359 is very compact with nanosized particles. The synthesis of Ni/Al LDH on this substrate generates a poorly  
360 resistant film, which tends to show grooves and cracks in the case of potentiostatic synthesis. With the  
361 potentiodynamic one, instead, spherical nanometric particles are observed. Thicknesses are around 1-1.5  $\mu\text{m}$   
362 for the potentiodynamic synthesis, while for the potentiostatic one they are around 700 nm. In general, the  
363 thickness values furtherly confirm that a lower amount of LDH is deposited with the potentiostatic method.  
364 For the supports characterized by the highest contact angles (CC and TC) the predominant morphology is the  
365 “desert rose”. This result is explicable with the weak interactions between the polar brucitic layers (which  
366 can be easily assumed similar to water) and the hydrophobic surface of these supports which induces a  
367 directional growth of the deposit toward the solution bulk.

368 As to the potentiodynamic approach, the deposits with the highest thickness are obtained when the support  
369 is NiF, while the thickness decreases in the following order: G, CC and TC (the latter two being similar).  
370 Thicknesses roughly estimated from SEM images are reported in Table 5. This result is in good agreement

371 with the current values recorded during LDH deposition: in fact, the current intensities are usually related to  
 372 the amount of material.

373 **Table 5** Thicknesses as estimated from SEM images

Substrate	LDH	Synthetic approach	Thickness (nm)
<b>G</b>	<b>Ni/Al</b>	<b>D</b>	450
		<b>S</b>	430
	<b>Co/Al</b>	<b>D</b>	1000
		<b>S</b>	400
<b>TC</b>	<b>Ni/Al</b>	<b>D</b>	1100
		<b>S</b>	770
	<b>Co/Al</b>	<b>D</b>	265
		<b>S</b>	235
<b>CC</b>	<b>Ni/Al</b>	<b>D</b>	400
		<b>S</b>	75
	<b>Co/Al</b>	<b>D</b>	960
		<b>S</b>	250
<b>NiF</b>	<b>Ni/Al</b>	<b>D</b>	1200
		<b>S</b>	988
	<b>Co/Al</b>	<b>D</b>	535
		<b>S</b>	410

374

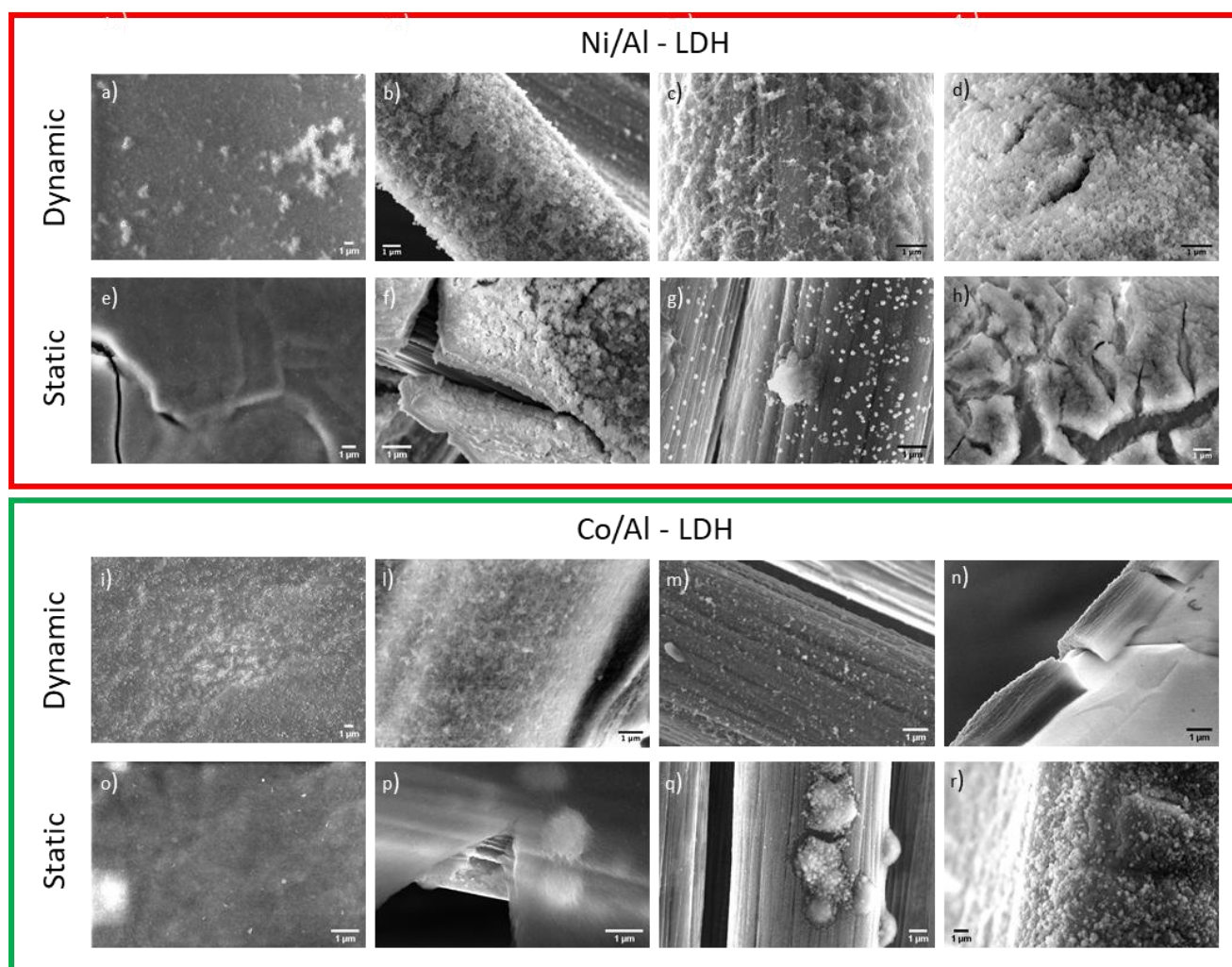
375 Elemental analysis was also carried out by EDS for all the electrosynthesized films (spectra not reported).  
 376 The presence of the expected elements (Co/Al/O and Ni/Al/O) plus carbon coming from the substrates was  
 377 observed.

Grafoil

Toray Carbon Paper

Carbon Cloth

Nickel Foam



378

379 **Figure 6.** SEM images the same indicated scale bar (1  $\mu\text{m}$ ). (a) Ni/Al-LDH\_D@G (b) Ni/Al-LDH\_D@TC (c) Ni/Al-  
 380 LDH \_D@CC (d) Ni/Al-LDH\_D@NiF. (e) Ni/Al-LDH\_S@G (f) Ni/Al-LDH\_S@TC (g) Ni/Al-LDH\_S@CC (h)  
 381 Ni/Al-LDH\_S@NiF. (i) Co/Al-LDH\_D@G (l) Co/Al-LDH\_D@TC (m) Co/Al-LDH\_D@CC (n) Co/Al-LDH\_D@NiF.  
 382 (o) Co/Al-LDH\_S@G (p) Co/Al-LDH\_S @TC (q) Co/Al-LDH\_S@CC (r) Co/Al-LDH\_S@NiF.

### 383 3.4. Raman Spectroscopy

384 The Raman spectra of the Co/Al and Ni/Al-LDH on the various substrates and for the two synthetic methods  
 385 are reported in Figure 7 in the wavenumber regions which allow for their identifications. The main spectral  
 386 features over the wavenumber range 200-1200  $\text{cm}^{-1}$  of the Co/Al LDH are the broad Raman shift at 472  $\text{cm}^{-1}$   
 387 <sup>1</sup>, with a shoulder at lower wavenumbers, and the sharper bands at 528 and 1050  $\text{cm}^{-1}$  (Fig. 7 a,c). Much  
 388 weaker features appear at 711  $\text{cm}^{-1}$  and below 300  $\text{cm}^{-1}$  (the latter assigned to lattice modes). Peak  
 389 assignments for this LDH have been widely discussed in the literature and we have recently reviewed them

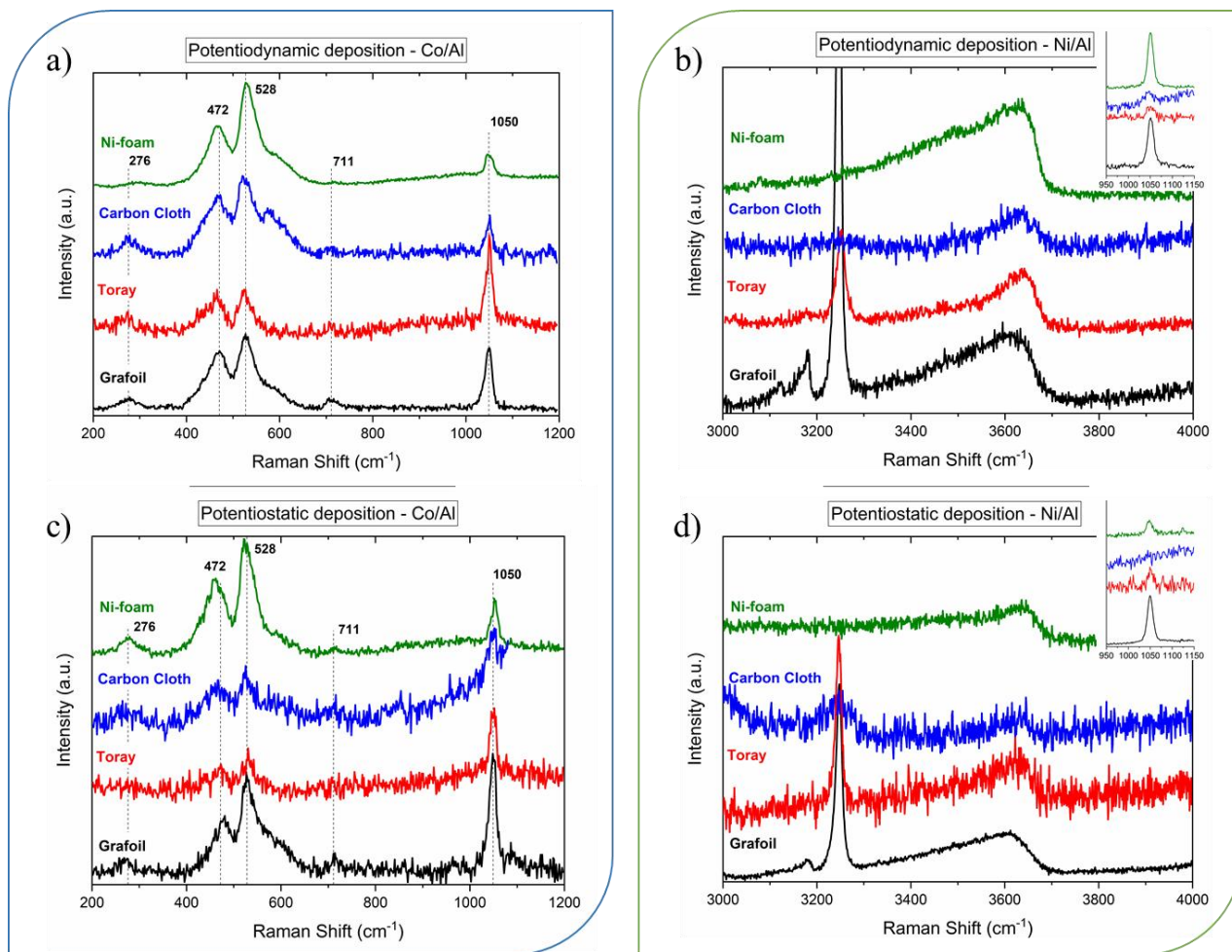
(Yang et al., 2017; Pérez-Ramírez et al., 2001; Klopogge et al., 2002; Musella et al., 2019b; Yang et al., 2010). The agreement with the data previously obtained confirms the chemical nature and the structural characteristics of the deposited material. (Musella et al., 2019b, 2019a)

The Raman spectrum of Ni/Al-LDH is generally much weaker over the entire energy range and its most relevant spectroscopic feature is the very broad band centered around  $3630\text{ cm}^{-1}$  (Fig. 7 b,d), in agreement with the literature findings, which corresponds to OH stretching of the  $\text{Ni}(\text{OH})_2$ . (Deabate et al., 2000) At lower wavenumbers, the only band observed is the nitrate stretching at  $1050\text{ cm}^{-1}$ , detected for all LDH with the exception of the sample obtained by the potentiostatic method on Carbon Cloth, as reported in the inset in Figure 7. Other spectral peaks are found to belong to the substrate.

We can conclude that, independently of the details of the spectral analysis, the Raman measurements efficiently probe the chemical identity of the materials obtained on all the four supports. Both for Co/Al and Ni/Al-LDH, the spectra on each substrate are virtually the same and, therefore, we can assume that the structure and the composition of the LDH do not depend on the nature of the support.

Generally, for a given support the Raman spectra of the samples prepared by potentiodynamic electrodeposition display a stronger intensity with respect to those obtained by the potentiostatic method. Although a quantitative estimate is not possible, such a behavior closely mirrors the findings of the morphology study, which suggests that the obtained film is thicker with a better degree of crystallinity, and the substrate is more homogeneously covered when the potentiodynamic approach is used. Nickel Foam and Grafoil are the substrates which yield the most intense Raman signal, again in agreement with the morphology results for those systems.

Infrared spectroscopy is also a widely used technique for the characterization of LDH, in particular for Ni-Al-LDH (Tonda et al., 2018, He et al., 2014, Ehlsissen et al., 1993). To further confirm the chemical nature of the electrodeposited materials, IR spectra were also recorded, and are reported with a discussion on bands assignments in SI 2.



415

416 **Figure 7.** Raman spectra of (a,c) Co/Al-LDH and (b,d) Ni/Al-LDH on Grafoil, Toray Carbon paper, Carbon Cloth and  
417 Nickel Foam.

### 418 3.5. Hybrid capacitor performances

419 In addition to the Faradaic process described in the first section, the charge storage characteristics of the  
420 films have been evaluated to demonstrate their possible application in hybrid electrochemical capacitors. The  
421 Ni/Al-LDH\_D@G system was selected as cathode. Grafoil as substrate ensures a high control of the film  
422 produced at the electrode and has been already employed by our group in different applications (Musella et  
423 al., 2019b, 2019a). The nickel based LDH has been chosen due to the deep knowledge on this material  
424 related to the many studies carried out in the past. Moreover, the use an electrode modified with a Ni based  
425 LDH is further justified by the necessity of limiting the use of Co in real devices, since it has become a  
426 critical constraint on the supply chain of the energy storage and conversion industry (Muralidharan et al.  
427 2020). As already stated, an electrosynthesized conductive polymer has been chosen as anode to obtain an  
428 all-binder-free system.



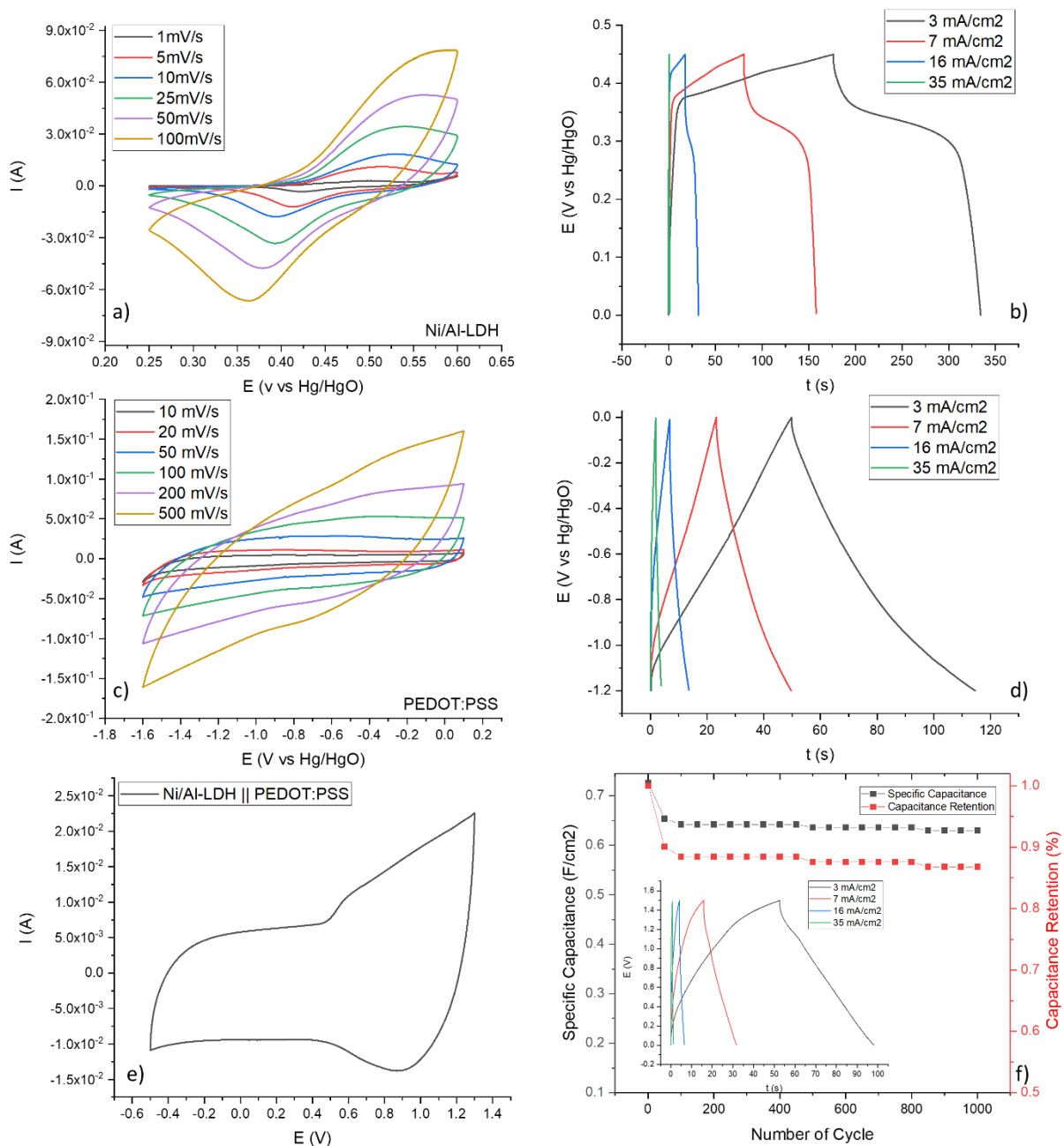
429 The electrochemical properties of the electrodes were investigated in a three-electrode cell using 6 M KOH  
430 as the supporting electrolyte. Figure 8a shows the CVs of the Ni/Al-LDH\_D@G recorded at different scan  
431 rates. The process can be considered dominated by a Faradaic reaction under diffusion control and the  
432 potential window is approximately 0.45 V wide, which is quite narrow for energy storage device  
433 development. Figure 8b shows the galvanostatic charge/discharge (GC-D) curves in the potential range 0–  
434 0.50 V. The LDH displays a response which is not only described with the classical plateau behavior derived  
435 from a Faradaic process but there is also a portion of the time in which the variation with potential is linear.  
436 The average specific capacitance calculated from the CVs is around 1.2 F/cm<sup>2</sup> (estimated to be around 550  
437 F/g). The capacitance can also be estimated starting from GC-D curves: it results 1.2, 0.6, 0.2 and 0.08 F/cm<sup>2</sup>  
438 at current densities of 3, 7.5, 16 and 35 mA/cm<sup>2</sup>, respectively. It can be noticed that the capacitance values  
439 decrease with the increase in current density: this is due to the sluggish electrolyte ions diffusion. It is worthy  
440 to highlight that a low ohmic drop can be observed when the current is reversed from charge to discharge due  
441 to the internal resistance.

442 In the case of PEDOT:PSS, both CVs (Figure 8c) and GC-D curves (Figure 8d) display a purely capacitive  
443 behavior in the potential range investigated, thus highlighting the charge storage capabilities. The average  
444 specific capacitance calculated from the CVs is 0.2 F/cm<sup>2</sup>. Considering the GC-D curves, the obtained values  
445 are 0.25, 0.23, 0.7 and 0.1 F/cm<sup>2</sup> at current densities of 3, 7.5, 16 and 35 mA/cm<sup>2</sup>, respectively.

446 Finally, Figures 8e, and f describe the configuration in solution, where the two electrodeposited electrodes  
447 were coupled and immersed in 6 M KOH under nitrogen, i.e., the cell configuration involved Ni/Al-LDH at  
448 one terminal side and PEDOT:PSS at the second one. The CV response is plotted in Figure 8e whilst Figure  
449 8f shows the evaluation of long-term stability. The C<sub>s</sub> calculated from CV results 0.67 F/cm<sup>2</sup>, whereas from  
450 GC-D curves the values are 0.73 0.52, 0.49 and 0.45 F/cm<sup>2</sup> at current densities of 3, 7.5, 16 and 35 mA/cm<sup>2</sup>,  
451 respectively. (inset). The capacitor has a starting discharge C<sub>s</sub> of 0.72 F/cm<sup>2</sup> which decreases and stabilizes at  
452 0.65 F/cm<sup>2</sup> after 20 cycles. The capacity retention is 86% after 1000 cycles (Figure 8f).

453 These preliminary data highlight that Ni/Al-LDH can be successfully deposited on a low-cost support, like  
454 Grafoil, which is highly compatible for supercapacitors applications. In particular, we propose a proof of

455 concept system able to embrace the necessity of sustainability: just earth abundant safe reagents, no binder  
 456 and watery solutions have been exploited.



457  
 458 **Figure 8** (a) characterization CV of Ni/Al-LDH\_D@G, (b) charge/discharge curves of Ni/Al-LDH\_D@G (c)  
 459 characterization CV of PEDOT:PSS@G (d) charge/discharge curves of PEDOT:PSS@G (e) characterization CV of  
 460 Ni/Al-LDH\_D@G || PEDOT:PSS@G, (f) long term stability test at 3 mA/cm<sup>2</sup> of Ni/Al-LDH\_D@G || PEDOT:PSS@G,  
 461 inset: charge/discharge curves at different current densities.

462

#### 463 4. Conclusions

464 Films of Co/Al and Ni/Al-LDH were prepared by two electrodeposition approaches onto four supports. The  
465 best films in terms of stability and reproducibility have been obtained through the potentiodynamic route;  
466 however, the most important observation is that the main contribution to the rate of the reactions involved in  
467 LDH precipitation is the nature of the electrode surface, independently of the adopted synthetic strategy. The  
468 most relevant result is that when the potentiodynamic approach is adopted, the substrate is homogeneously  
469 covered, and no detachment of the film is highlighted in any case, as can be seen by SEM. Otherwise for the  
470 potentiostatic synthesis, the deposit shows breakages and detachments. Raman characterizations confirm the  
471 LDH structure of the electrosynthesized materials.

472 Finally, the specific capacitance of the Ni/Al LDH was evaluated and resulted  $1.2 \text{ F/cm}^2$  which is a value that  
473 makes the material a good candidate for the development of supercapacitors devices. Therefore, as a proof of  
474 concept, a two terminal device was tested, using LDH as cathode and PEDOT:PSS as anode, which  
475 displayed a calculated capacitance by charge/discharge curves of almost  $0.7 \text{ F/cm}^2$ . The most outstanding  
476 result is that no harmful substances, no binders and water solutions have been employed, and thus the  
477 proposed application goes towards a sustainable chemistry.

478 **4. Author Contributions:** E. M. wrote the article and analyzed the data. E.M. and I. G. performed the  
479 experiments. I.G. designed the device. E.M., I.G. and D.T. designed the methodology. F.C., M.C. and V.M.  
480 performed and analyzed SEM and EDS data. A.R. and E.V. performed and analyzed Raman and IR spectra.  
481 D.T. supervised the research project and decided the resource goals and aims. D.T., F.B., and M.G. funded  
482 the resource. All the authors discussed the results and revised the text.

483 **5. Funding:** This research was funded by The European Union's Horizon 2020 Research and Innovation  
484 Program (Grant Agreement no. 881603 GrapheneCore3 Graphene Flagship) and by Italian Ministry of  
485 Research (MIUR) within PRIN-2015 Project no. NEWLI2015CL3APH.

486 **6. Acknowledgments:** The authors are grateful to the University of Bologna, Italy for providing financial  
487 support. Thanks are also due to Alessandro Calvise and Giacomo Ferrari for performing part of the  
488 electrochemical tests. Thanks are also due to Andrea Giunchi for the help in analyzing IR spectra.

## 489 7. References

- 490 Adachi-pagano, M., Forano, C., Besse, J., Mate, L., No, C., Pascal, B., 2003. Synthesis of Al-rich  
491 hydrotalcite-like compounds by using the urea hydrolysis reaction — control of size and morphology.  
492 <https://doi.org/10.1039/b302747n>
- 493 Asiabi, H., Yamini, Y., Alipour, M., Shamsayei, M., Hosseinkhani, S., 2019. Synthesis and characterization  
494 of a novel biocompatible pseudo-hexagonal NaCa-layered double metal hydroxides for smart pH-  
495 responsive drug release of dacarbazine and enhanced anticancer activity in malignant melanoma.  
496 *Mater. Sci. Eng. C* 97, 96–102. <https://doi.org/10.1016/j.msec.2018.12.017>
- 497 Benito, P., Monti, M., De Nolf, W., Nuyts, G., Janssen, G., Fornasari, G., Scavetta, E., Basile, F., Janssens,  
498 K., Ospitali, F., Tonelli, D., Vaccari, A., 2015. Improvement in the coating homogeneity in  
499 electrosynthesized Rh structured catalysts for the partial oxidation of methane. *Catal. Today* 246, 154–  
500 164. <https://doi.org/10.1016/j.cattod.2014.10.003>
- 501 Bernardi, E., Monti, M., Tonelli, D., Ho, P.H., Benito, P., Vaccari, A., Nobili, L., Fornasari, G., Scavetta, E.,  
502 2016. Reactions involved in the electrodeposition of hydrotalcite-type compounds on FeCrAlloy foams  
503 and plates. *Electrochim. Acta* 222, 1335–1344. <https://doi.org/10.1016/j.electacta.2016.11.109>
- 504 Brasquet, C., Rousseau, B., Estrade-Szwarckopf, H., Le Cloirec, P., 2000. Observation of activated carbon  
505 fibres with SEM and AFM correlation with adsorption data in aqueous solution. *Carbon N. Y.* 38, 407–  
506 422. [https://doi.org/10.1016/S0008-6223\(99\)00120-7](https://doi.org/10.1016/S0008-6223(99)00120-7)
- 507 Cavani, F., Trifirò, F., Vaccari, A., 1991. Hydrotalcite-type anionic clays: preparation, properties and  
508 applications. *Catal. Today* 11, 173–301. <https://doi.org/10.1007/BF03263563>
- 509 Conte, M., Prosini, P.P., Passerini, S., 2004. Overview of energy/hydrogen storage: State-of-the-art of the  
510 technologies and prospects for nanomaterials. *Mater. Sci. Eng. B Solid-State Mater. Adv. Technol.* 108,  
511 2–8. <https://doi.org/10.1016/j.mseb.2003.10.107>
- 512 Cuesta, A., Dhamelincourt, P., Laureyns, J., Martinez-Alonso, A., & Tascón, J. D. (1994). Raman  
513 microprobe studies on carbon materials. *Carbon*, 32 (8), 1523–1532. [https://doi.org/10.1016/0008-6223\(94\)90148-1](https://doi.org/10.1016/0008-6223(94)90148-1)  
514

515 Deabate, S., Fourgeot, F., Henn, F., 2000. X-ray diffraction and micro-Raman spectroscopy analysis of new  
 516 nickel hydroxide obtained by electrodialysis. *J. Power Sources* 87, 125–136.  
 517 [https://doi.org/10.1016/S0378-7753\(99\)00437-1](https://doi.org/10.1016/S0378-7753(99)00437-1)

518 Ehlsissen, K. T., Delahaye-Vidal, A., Genin, P., Figlarz, M., & Willmann, P. (1993). Preparation and  
 519 characterization of turbostratic Ni/Al layered double hydroxides for nickel hydroxide electrode  
 520 applications. *J. Mat. Chem.*, 3, 8, 883-888. <https://doi.org/10.1039/JM9930300883>

521 Erickson, K.L., Bostrom, T.E., Frost, R.L., 2005. A study of structural memory effects in synthetic  
 522 hydrotalcites using environmental SEM 59, 226–229. <https://doi.org/10.1016/j.matlet.2004.08.035>

523 Ferrari, A. C., Basko, D. M., 2013. Raman spectroscopy as a versatile tool for studying the properties of  
 524 graphene. *Nature nanotechnology* 8.4, 235-246. <https://doi.org/10.1038/nnano.2013.46>

525 Gualandi, I., Scavetta, E., Vlamidis, Y., Casagrande, A., Tonelli, D., 2015. Co/Al layered double hydroxide  
 526 coated electrode for in flow amperometric detection of sugars. *Electrochim. Acta* 173, 67–75.  
 527 <https://doi.org/10.1016/j.electacta.2015.04.172>

528 Gualandi, I., Scavetta, E., Zappoli, S., Tonelli, D., 2011. Electrocatalytic oxidation of salicylic acid by a  
 529 cobalt hydrotalcite-like compound modified Pt electrode. *Biosens. Bioelectron.* 26, 3200–3206.  
 530 <https://doi.org/10.1016/j.bios.2010.12.026>

531 Gualandi, I., Solito, A.G., Scavetta, E., Tonelli, D., 2012. Electrochemical Pretreatment of Pt Surface:  
 532 Modification with Co/Al Layered Double Hydroxide for Analytical Applications. *Electroanalysis* 24,  
 533 857–864. <https://doi.org/10.1002/elan.201100567>

534 Gualandi, I., Vlamidis, Y., Mazzei, L., Musella, E., Giorgetti, M., Christian, M., Morandi, V., Scavetta, E.,  
 535 Tonelli, D., 2019. Ni/Al Layered Double Hydroxide and Carbon Nanomaterial Composites for Glucose  
 536 Sensing. *ACS Appl. Nano Mater.* 2, 143–155. <https://doi.org/10.1021/acsanm.8b01765>

537 Hareesh, K., Shateesh, B., Joshi, R.P., Dahiwal, S.S., Bhoraskar, V.N., Haram, S.K., Dhole, S.D., 2016.  
 538 PEDOT:PSS wrapped NiFe<sub>2</sub>O<sub>4</sub>/rGO tertiary nanocomposite for the super-capacitor applications.  
 539 *Electrochim. Acta* 201, 106–116. <https://doi.org/10.1016/j.electacta.2016.03.205>

540 He, F., Hu, Z., Liu, K., Zhang, S., Liu, H., Sang, S. 2014. In situ fabrication of nickel aluminum-layered  
 541 double hydroxide nanosheets/hollow carbon nanofibers composite as a novel electrode material for  
 542 supercapacitors. *J. of Power Sources*, 267, 188-196. <https://doi.org/10.1016/j.jpowsour.2014.05.084>

543 He, J., Wei, M., Li, B., Kang, Y., Evans, D.G., Duan, X., 2006. Preparation of layered double hydroxides.  
 544 *Layer. Double Hydroxides* 119, 89–119. [https://doi.org/10.1007/430\\_006](https://doi.org/10.1007/430_006)

545 Jorio, A., Souza Filho, A. G., 2016. Raman studies of carbon nanostructures. *Annual Review of Materials*  
 546 *Research* 46, 357-382. <https://doi.org/10.1146/annurev-matsci-070115-032140>

547 Khan, A.I., O'Hare, D., 2002. Intercalation chemistry of layered double hydroxides: Recent developments  
 548 and applications. *J. Mater. Chem.* 12, 3191–3198. <https://doi.org/10.1039/b204076j>

549 Kloprogge, J.T., Wharton, D., Hickey, L., Frost, R.L., 2002. Infrared and Raman study of interlayer anions  
 550 CO<sub>3</sub> in Mg / Al- hydrotalcite. *Am. Mineral.* 87, 623–629. <https://doi.org/0003-004X/02/0506>

551 Konopa, S.J., McDuffie B., (1970) Diffusion coefficients of ferri- and ferrocyanide ions in aqueous media,  
 552 using twin-electrode thin-layer electrochemistry *Anal. Chem.*, 42, 1741-1746.  
 553 <https://doi.org/10.1021/ac50160a042>

554 McCrory, C.C.L., Jung, S., Peters, J.C., Jaramillo, T.F., 2013. Benchmarking heterogeneous electrocatalysts  
 555 for the oxygen evolution reaction. *J. Am. Chem. Soc.* 135, 16977–16987.  
 556 <https://doi.org/10.1021/ja407115p>

557 McCrory, C.C.L.L., Jung, S., Ferrer, I.M., Chatman, S.M., Peters, J.C., Jaramillo, T.F., 2015. Benchmarking  
 558 Hydrogen Evolving Reaction and Oxygen Evolving Reaction Electrocatalysts for Solar Water Splitting  
 559 Devices. *J. Am. Chem. Soc.* 137, 4347–4357. <https://doi.org/10.1021/ja510442p>

560 Meyer, P.D.T.J., Sauvage, H.W.R.J., 2005. Layered Double Hydroxides, Structure and Bonding.  
 561 <https://doi.org/10.1007/b100426>

562 Miller, J.R., Simon, P., 2008. Electrochemical Capacitors for. *Science* (80-. ). 321, 651–652.  
 563 <https://doi.org/10.1126/science.1158736>

564 Miyata, S., 1983. Anion-Exchange Properties of Hydrotalcite-Like Compounds. *Clays Clay Miner.* 31, 305–

565 311. <https://doi.org/10.1346/CCMN.1983.0310409>

566 Morishita, M., 2011. Surface observation and magnetization measurements of Grafoil substrate. *J. Low*  
567 *Temp. Phys.* 162, 638–644. <https://doi.org/10.1007/s10909-010-0328-7>

568 Muralidharan, N., Essehli, R., Hermann R.P., Amin R., Jafta C., Zhang, J., Liu, J., Du, Z., Meyer, H.M., Self,  
569 E., Nanda, J., Belharouak, I., 2020. Lithium Iron Aluminum Nickelate,  $\text{LiNi}_{0.5}\text{Fe}_{0.5}\text{Al}_2\text{O}_7$ —New  
570 Sustainable Cathodes for Next-Generation Cobalt-Free Li-Ion Batteries, *Adv. Mater.* 32 (34), 2002960.  
571 <https://doi.org/10.1002/adma.202002960>.

572 Musella, E., Gualandi, I., Scavetta, E., Gazzano, M., Rivalta, A., Venuti, E., Christian, M., Morandi, V.,  
573 Tonelli, D., 2019a. Electrochemical Approach for the Production of Layered Double Hydroxides with a  
574 Well-Defined Co/MeIII Ratio. *Chem. - A Eur. J.* 25, 16301–16310.  
575 <https://doi.org/10.1002/chem.201903288>

576 Musella, E., Gualandi, I., Scavetta, E., Rivalta, A., Venuti, E., Christian, M., Morandi, V., Mullaliu, A.,  
577 Giorgetti, M., Tonelli, D., 2019b. Newly developed electrochemical synthesis of Co-based layered  
578 double hydroxides: Toward noble metal-free electro-catalysis. *J. Mater. Chem. A* 7, 11241–11249.  
579 <https://doi.org/10.1039/c8ta11812d>

580 Nalawade, P., Aware, B., Kadam, V.J., Hirlekar, R.S., 2009. Layered double hydroxides : A review 68, 267–  
581 272.

582 Ogawa, M., Asai, S., 2000. Hydrothermal Synthesis of Layered Double Hydroxide - Deoxycholate  
583 Intercalation 3253–3255. <https://doi.org/10.1021/cm000455n>

584 Pérez-Ramírez, J., Mul, G., Kapteijn, F., Moulijn, J.A., 2001. In situ investigation of the thermal  
585 decomposition of Co–Al hydrotalcite in different atmospheres. *J. Mater. Chem.* 11, 821–830.  
586 <https://doi.org/10.1039/b009320n>

587 Prevot, V., Caperaa, N., Taviot-gue, C., Forano, C., 2009. Glycine-Assisted Hydrothermal Synthesis of  
588 NiAl-Layered Double Hydroxide Nanostructures & DESIGN 2009.

589 Scavetta, E., Ballarin, B., Corticelli, C., Gualandi, I., Tonelli, D., Prevot, V., Forano, C., Mousty, C., 2012.

590 An insight into the electrochemical behavior of Co/Al layered double hydroxide thin films prepared by  
 591 electrodeposition. *J. Power Sources* 201, 360–367. <https://doi.org/10.1016/j.jpowsour.2011.10.122>

592 Scavetta, E., Ballarin, B., Giorgetti, M., Carpani, I., Cogo, F., Tonelli, D., 2004. Electrodes modified by One-  
 593 Step Electrosynthesis of Ni/Al-NO<sub>3</sub> Double Layered Hydroxide. *J. New Mater. Electrochem. Syst.* 7,  
 594 43–50.

595 Scavetta, E., Casagrande, A., Gualandi, I., Tonelli, D., 2014a. Analytical performances of Ni LDH films  
 596 electrochemically deposited on Pt surfaces: Phenol and glucose detection. *J. Electroanal. Chem.* 722–  
 597 723, 15–22. <https://doi.org/10.1016/j.jelechem.2014.03.018>

598 Scavetta, E., Gualandi, I., Tonelli, D., Mousty, C., Prevot, V., Monti, M., 2014b. Electrodeposition of  
 599 Layered Double Hydroxides on platinum: Insights into the reactions sequence. *Electrochim. Acta* 152,  
 600 75–83. <https://doi.org/10.1016/j.electacta.2014.11.096>

601 Su, W., Roy, D. 2013. Visualizing graphene edges using tip-enhanced Raman spectroscopy. *Journal of*  
 602 *Vacuum Science & Technology B* 31, 4, 1808. <https://doi.org/10.1116/1.4813848>.

603 Totir, D., Mo, Y., Kim, S., Antonio, M.R., Scherson, D.A., 2000. In Situ Co K-Edge X-Ray Absorption Fine  
 604 Structure of Cobalt Hydroxide Film Electrodes in Alkaline Solutions. *J. Electrochem. Soc.* 147, 4594.  
 605 <https://doi.org/10.1149/1.1394107>

606 Tonda, S., Kumar, S., Bhardwaj, M., Yadav, P., Ogale, S., 2018. g-C<sub>3</sub>N<sub>4</sub>/NiAl-LDH 2D/2D hybrid  
 607 heterojunction for high-performance photocatalytic reduction of CO<sub>2</sub> into renewable fuels. *ACS*  
 608 *applied materials & interfaces*, 10, 3, 2667-2678. <https://doi.org/10.1021/acsami.7b18835>

609 Vlamidis, Y., Lanzi, M., Salatelli, E., Gualandi, I., Fraboni, B., Setti, L., Tonelli, D., 2015. Electrodeposition  
 610 of PEDOT perchlorate as an alternative route to PEDOT:PSS for the development of bulk  
 611 heterojunction solar cells. *J. Solid State Electrochem.* 19, 1685–1693. [https://doi.org/10.1007/s10008-](https://doi.org/10.1007/s10008-015-2802-2)  
 612 [015-2802-2](https://doi.org/10.1007/s10008-015-2802-2)

613 Vlamidis, Y., Scavetta, E., Giorgetti, M., Sangiorgi, N., Tonelli, D., 2017. Electrochemically synthesized  
 614 cobalt redox active layered double hydroxides for supercapacitors development. *Appl. Clay Sci.* 143,  
 615 151–158. <https://doi.org/10.1016/j.clay.2017.03.031>



616 Yang, F., Sliozberg, K., Sinev, I., Antoni, H., Bähr, A., Ollegott, K., Xia, W., Masa, J., Grünert, W., Cuenya,  
 617 B.R., Schuhmann, W., Muhler, M., 2017. Synergistic Effect of Cobalt and Iron in Layered Double  
 618 Hydroxide Catalysts for the Oxygen Evolution Reaction. *ChemSusChem* 10, 156–165.  
 619 <https://doi.org/10.1002/cssc.201601272>

620 Yang, G.W., Xu, C.L., Li, H.L., 2008. Electrodeposited nickel hydroxide on nickel foam with ultrahigh  
 621 capacitance. *Chem. Commun.* 6537–6539. <https://doi.org/10.1039/b815647f>

622 Yang, J., Liu, H., Martens, W.N., Frost, R.L., 2010. Synthesis and characterization of Cobalt hydroxide,  
 623 cobalt oxyhydroxide, and cobalt oxide nanodiscs. *J. Phys. Chem. C* 114, 111–119.  
 624 <https://doi.org/10.1021/jp908548f>

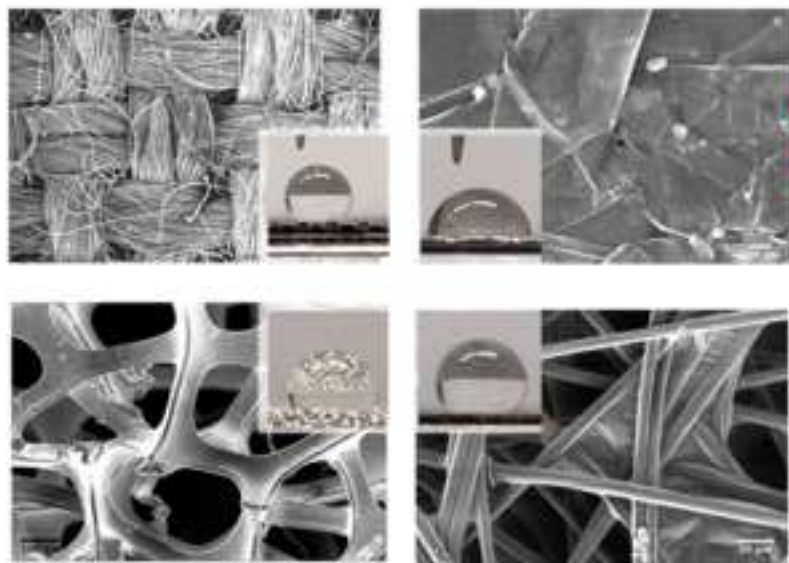
625 Yang, W., Gao, Z., Wang, J., Ma, J., Zhang, M., Liu, L., 2013. Solvothermal one-step synthesis of Ni-Al  
 626 layered double hydroxide/carbon nanotube/reduced graphene oxide sheet ternary nanocomposite with  
 627 ultrahigh capacitance for supercapacitors. *ACS Appl. Mater. Interfaces* 5, 5443–5454.  
 628 <https://doi.org/10.1021/am4003843>

629 Zamel, N., Li, X., Shen, J., 2009. Correlation for the effective gas diffusion coefficient in carbon paper  
 630 diffusion media. *Energy and Fuels* 23, 6070–6078. <https://doi.org/10.1021/ef900653x>

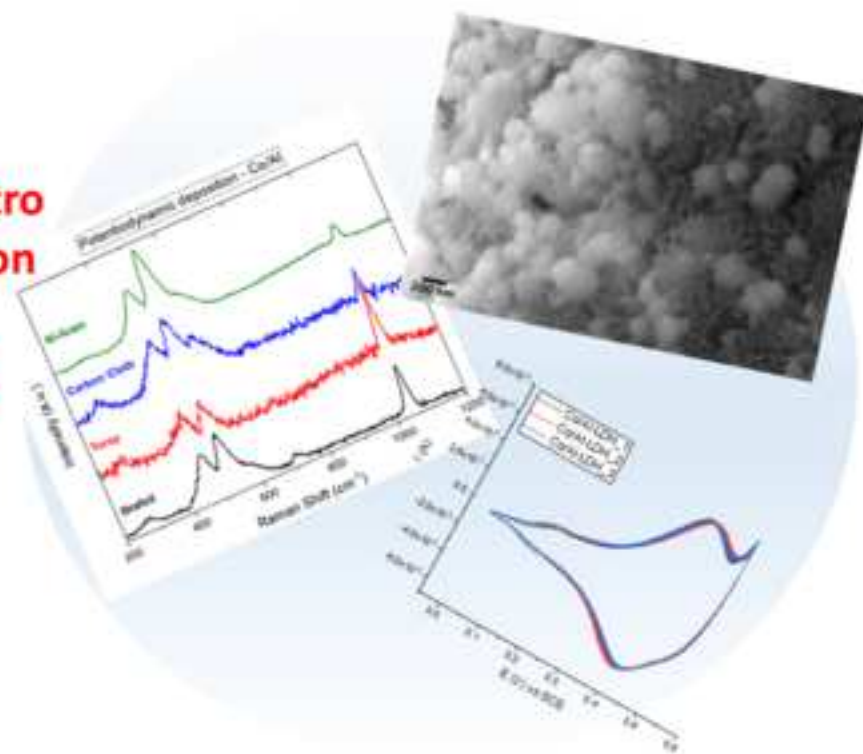
631 Zhang, L., Hui, K.N., Hui, K.S., Lee, H., 2015. Facile synthesis of porous CoAl-layered double  
 632 hydroxide/graphene composite with enhanced capacitive performance for supercapacitors. *Electrochim.*  
 633 *Acta* 186, 522–529. <https://doi.org/10.1016/j.electacta.2015.11.024>

634 Zhang, Y., Wei, S., 2019. Mg-Co-Al-LDH nanoparticles with attractive electrochemical performance for  
 635 supercapacitor. *J. Nanoparticle Res.* 21. <https://doi.org/10.1007/s11051-018-4452-7>

636



LDH electro  
deposition

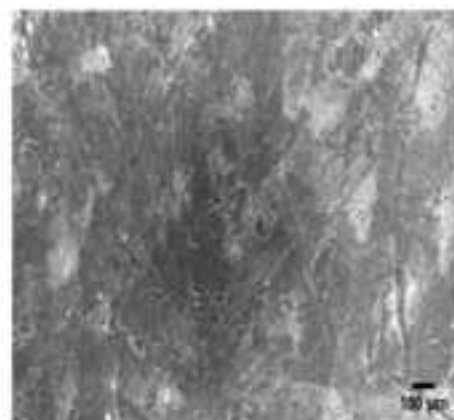
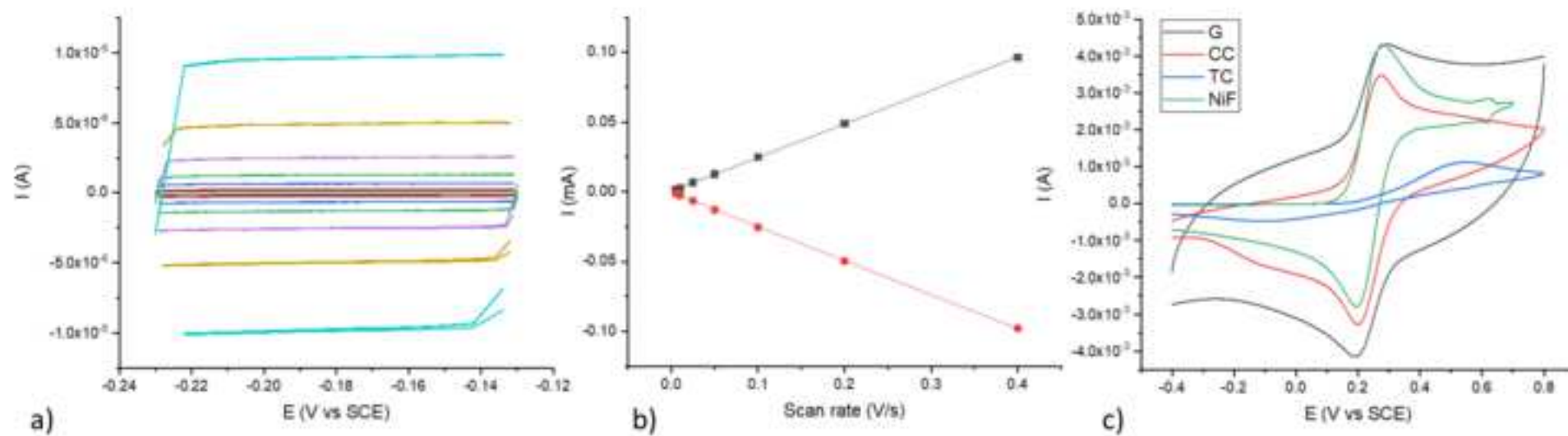


## **Highlights**

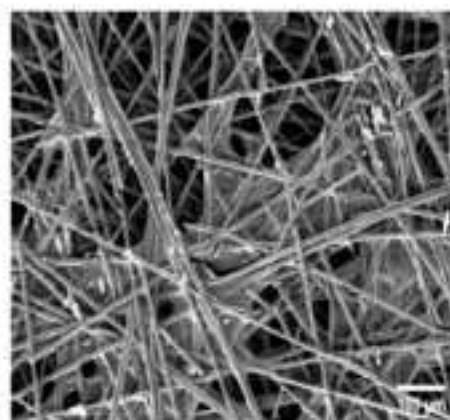
- Layered Double Hydroxides (LDHs) were electrochemically deposited on four supports
- Potentiostatic and potentiodynamic approaches were employed
- LDHs were characterized by SEM, Raman spectroscopy and electrochemical techniques
- Ni/Al LDH was evaluated as cathode material in hybrid supercapacitor (H-SC)
- An all-binder-free, aqueous and environmentally friendly H-SC was fabricated

Figure 2

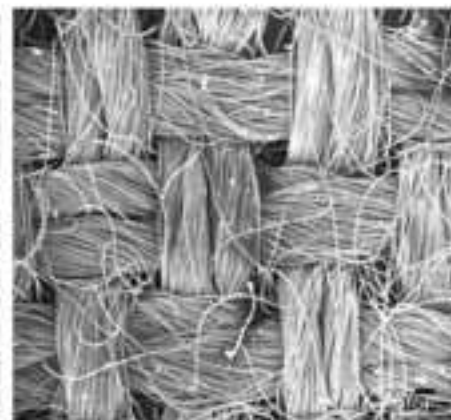
[Click here to download high resolution image](#)



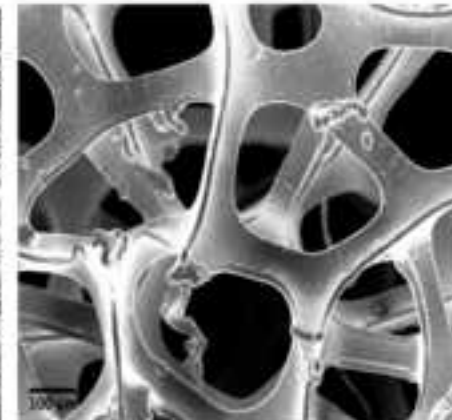
d) Grafoil



e) Toray Carbon Paper



f) Carbon Cloth



g) Nickel Foam

Figure 3

[Click here to download high resolution image](#)

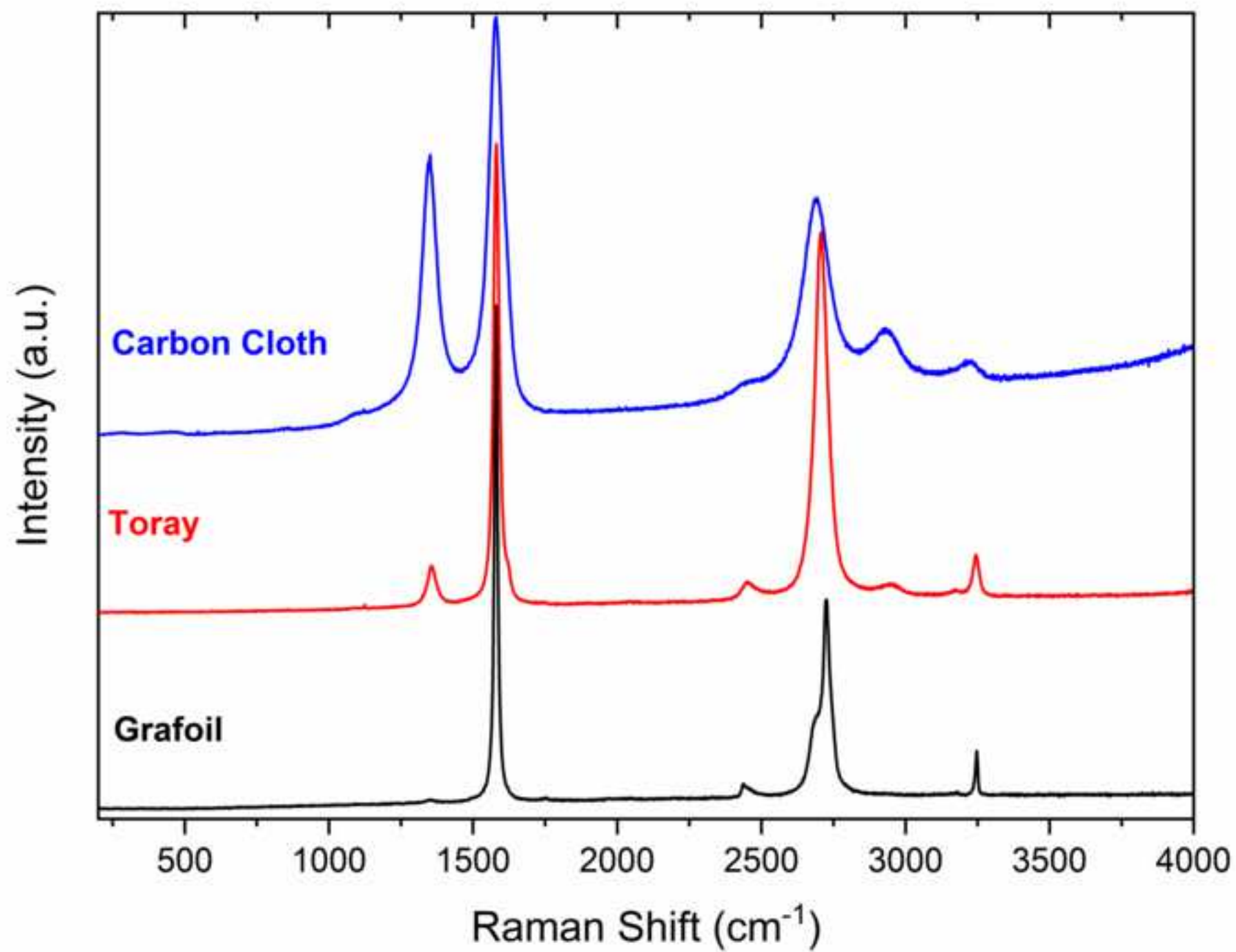


Figure 4

[Click here to download high resolution image](#)

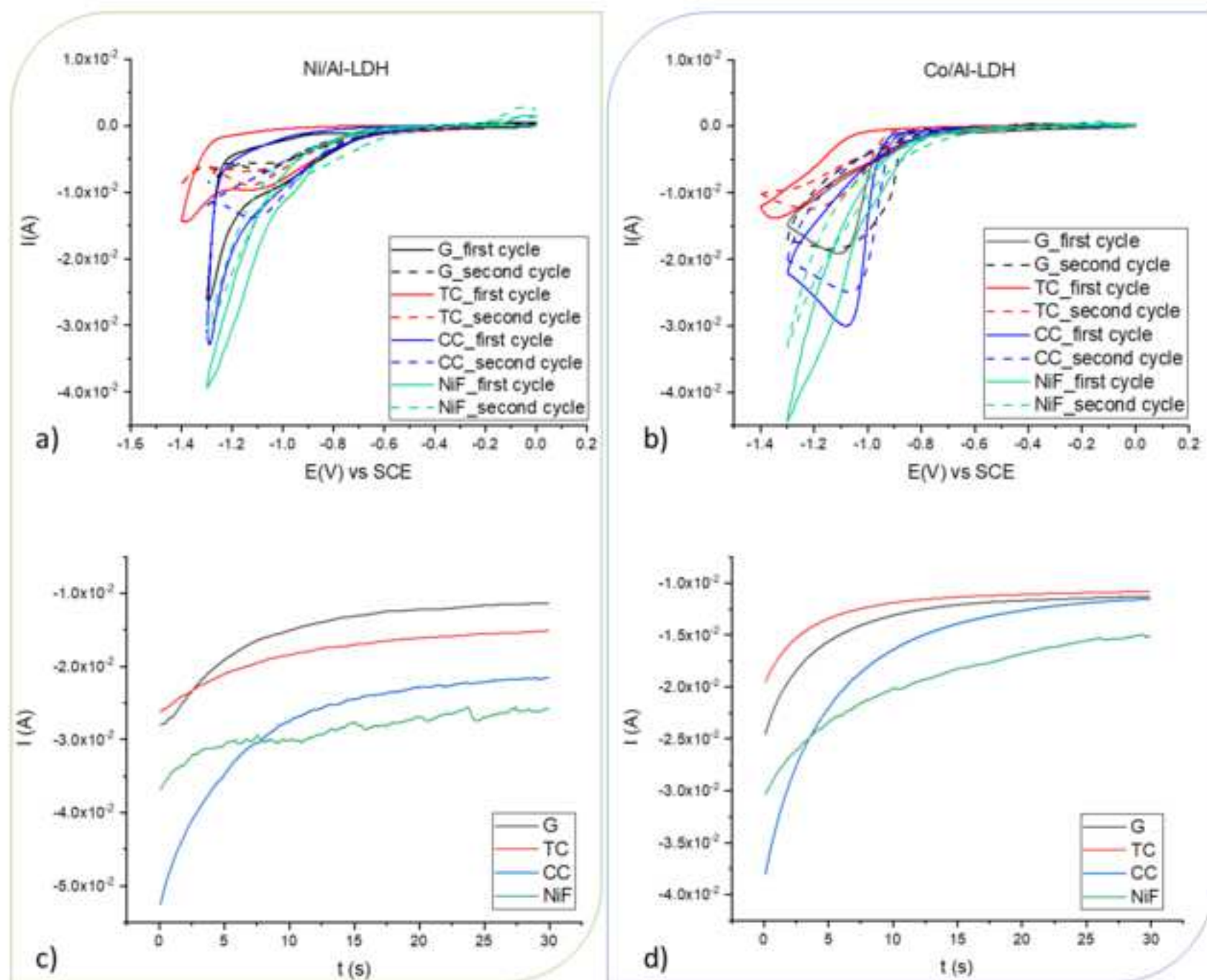




Figure 5  
[Click here to download high resolution image](#)

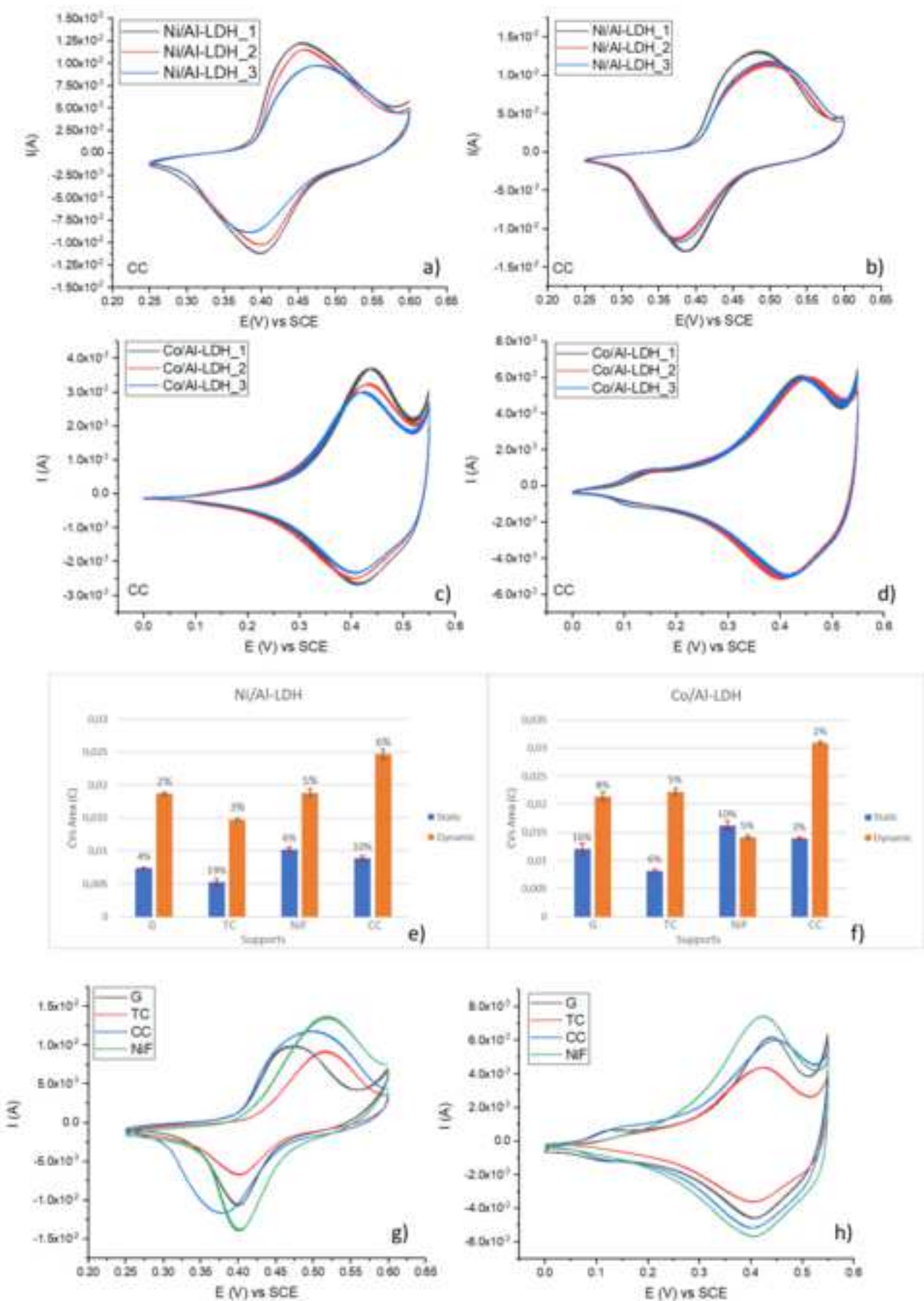
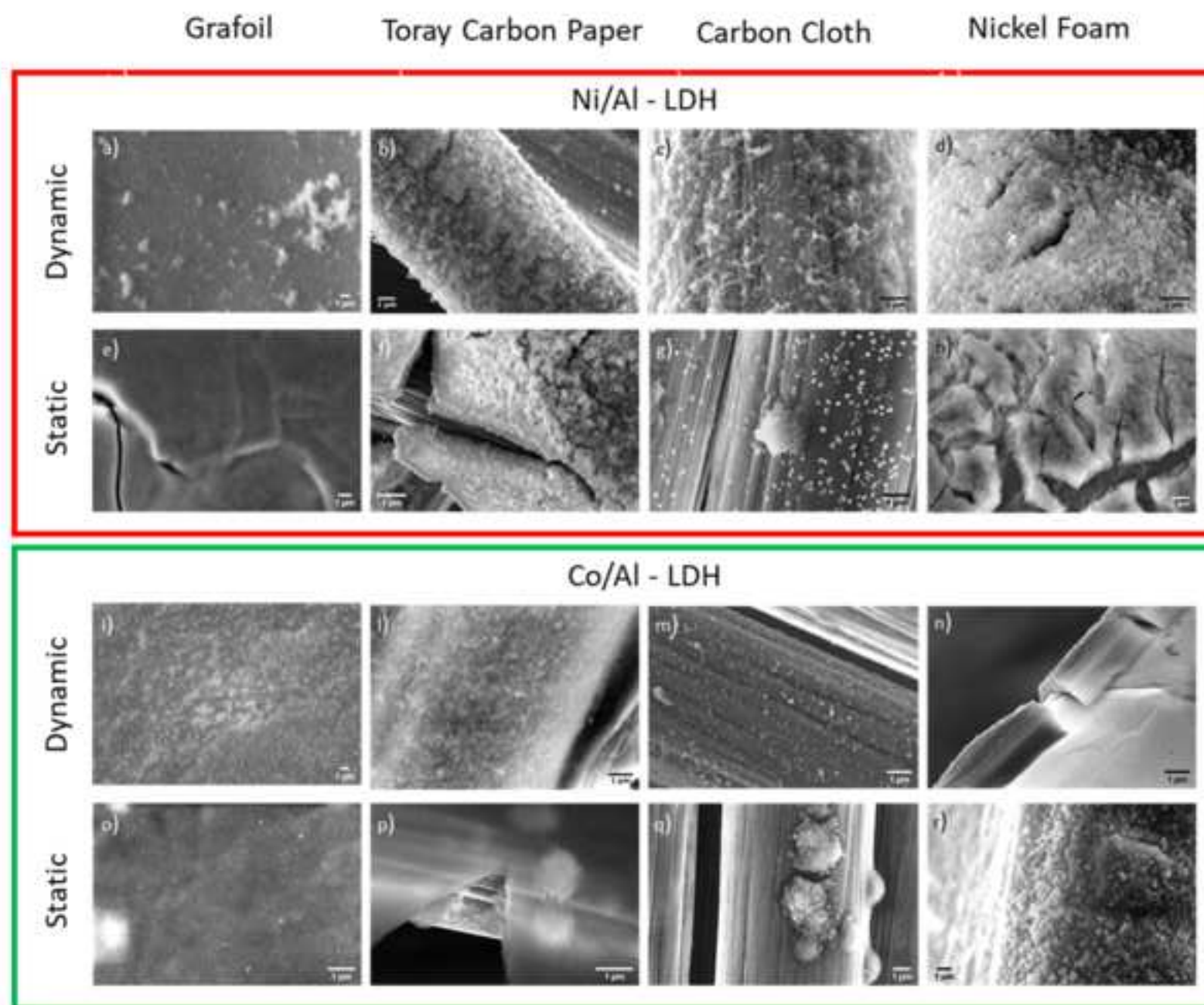


Figure 6

[Click here to download high resolution image](#)





**Figure 7**  
[Click here to download high resolution image](#)

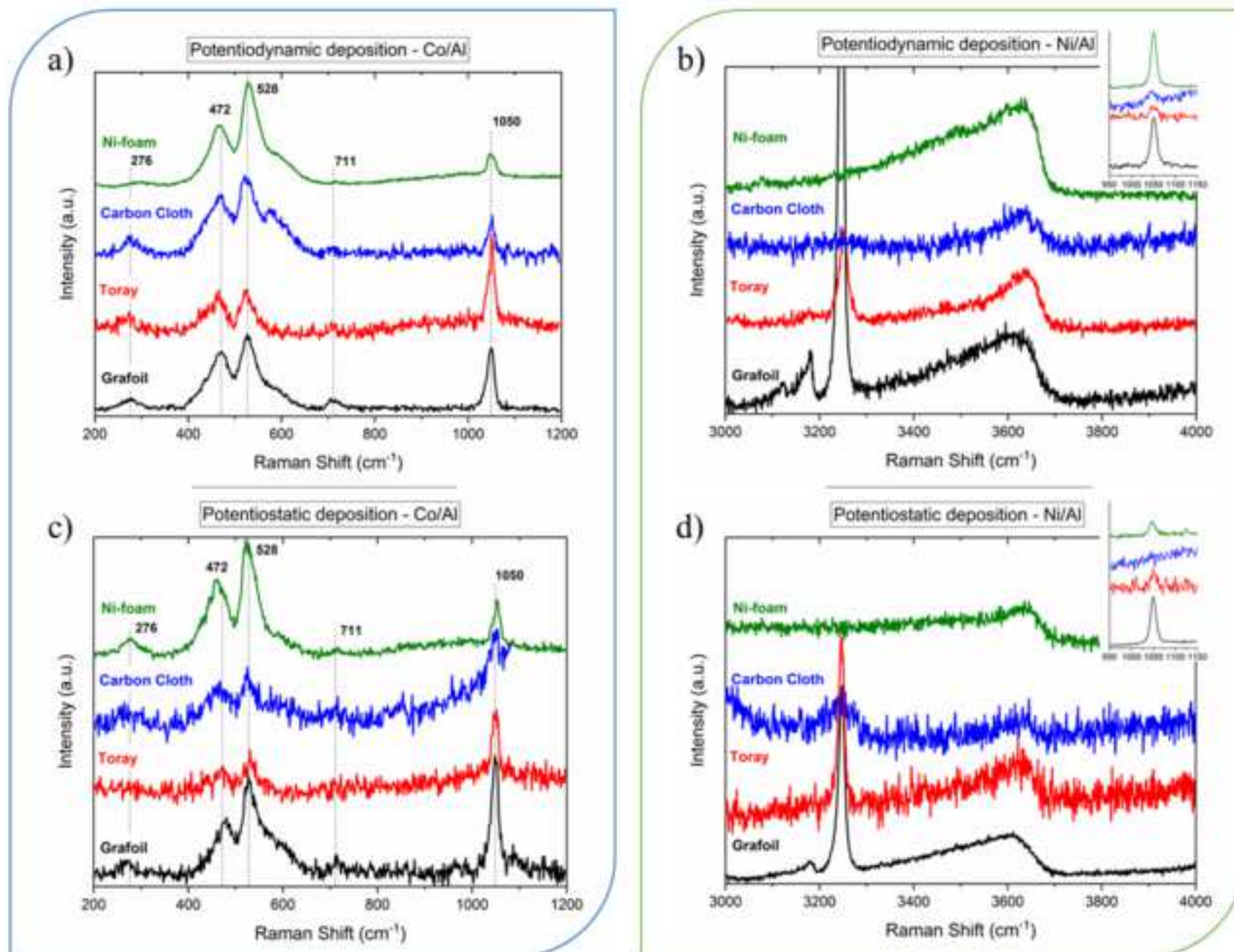


Figure 8  
[Click here to download high resolution image](#)

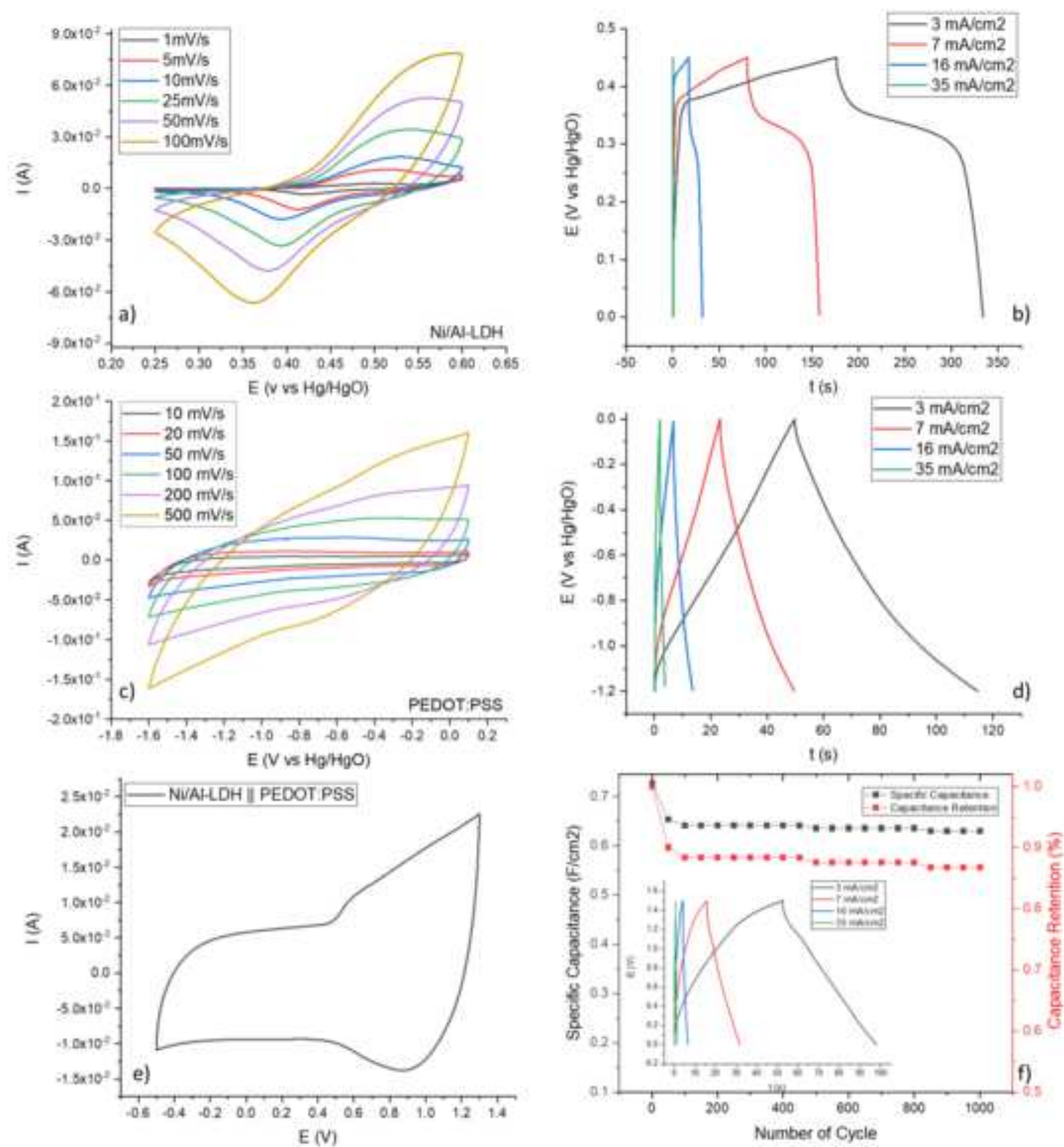
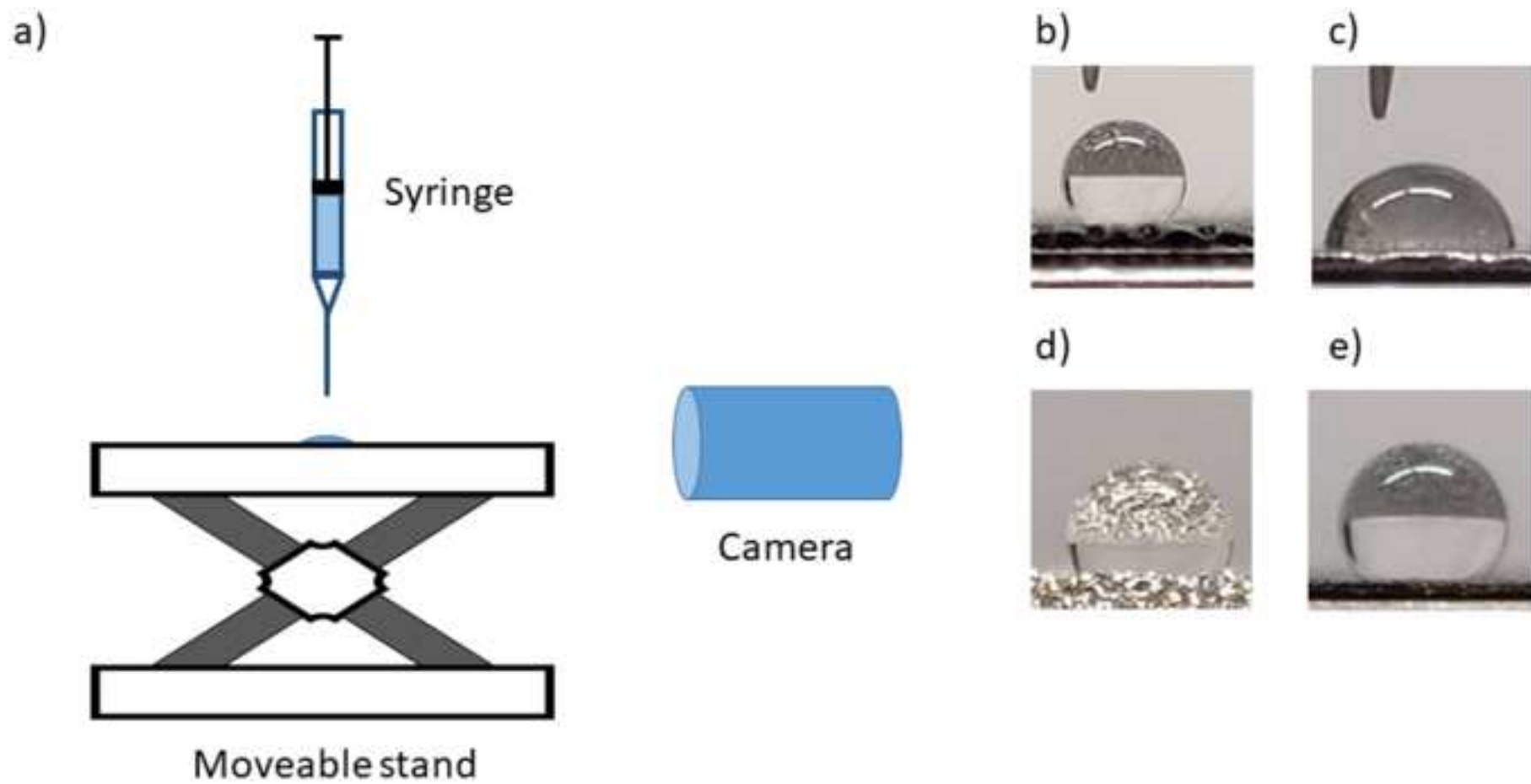


Figure 1  
[Click here to download high resolution image](#)



## Abstract

Thin films of Al, and Co or Ni based Layered Double Hydroxides (LDH) have been electrochemically deposited on four different supports (Grafoil, Toray Carbon Paper, Carbon Cloth and Nickel Foam) through a potentiostatic or a potentiodynamic approach. The obtained films have been fully characterized to compare their properties in dependence on the different deposition techniques and substrates. Finally, the Grafoil support modified with a Ni /Al-LDH has been employed as cathode in combination with a Grafoil anode modified with poly(3,4-ethylenedioxythiophene)-poly(styrenesulfonate) (PEDOT:PSS) also electrosynthesized, in order to develop an all-binder-free hybrid supercapacitor as a proof of concept to demonstrate the applicability in the field of energy storage.

**Supplementary Interactive Plot Data (CSV)**  
[Click here to download Supplementary Interactive Plot Data \(CSV\): SI final .docx](#)

**Declaration of interests**

☒ The authors declare that they have no known competing financial interests or personal relationships that could have appeared to influence the work reported in this paper.

☐ The authors declare the following financial interests/personal relationships which may be considered as potential competing interests:

## Credit Author Statement

E. M. wrote the article and analyzed the data. E.M. and I. G. performed the experiments. I.G. designed the device. E.M., I.G. and D.T. designed the methodology. F.C., M.C. and V.M. performed and analyzed SEM and EDS data. A.R. and E.V. performed and analyzed Raman and IR spectra. D.T. supervised the research project and decided the resource goals and aims. D.T. and M.G. funded the resource. All the authors discussed the results and revised the text.